SELENOLOGY TODAY

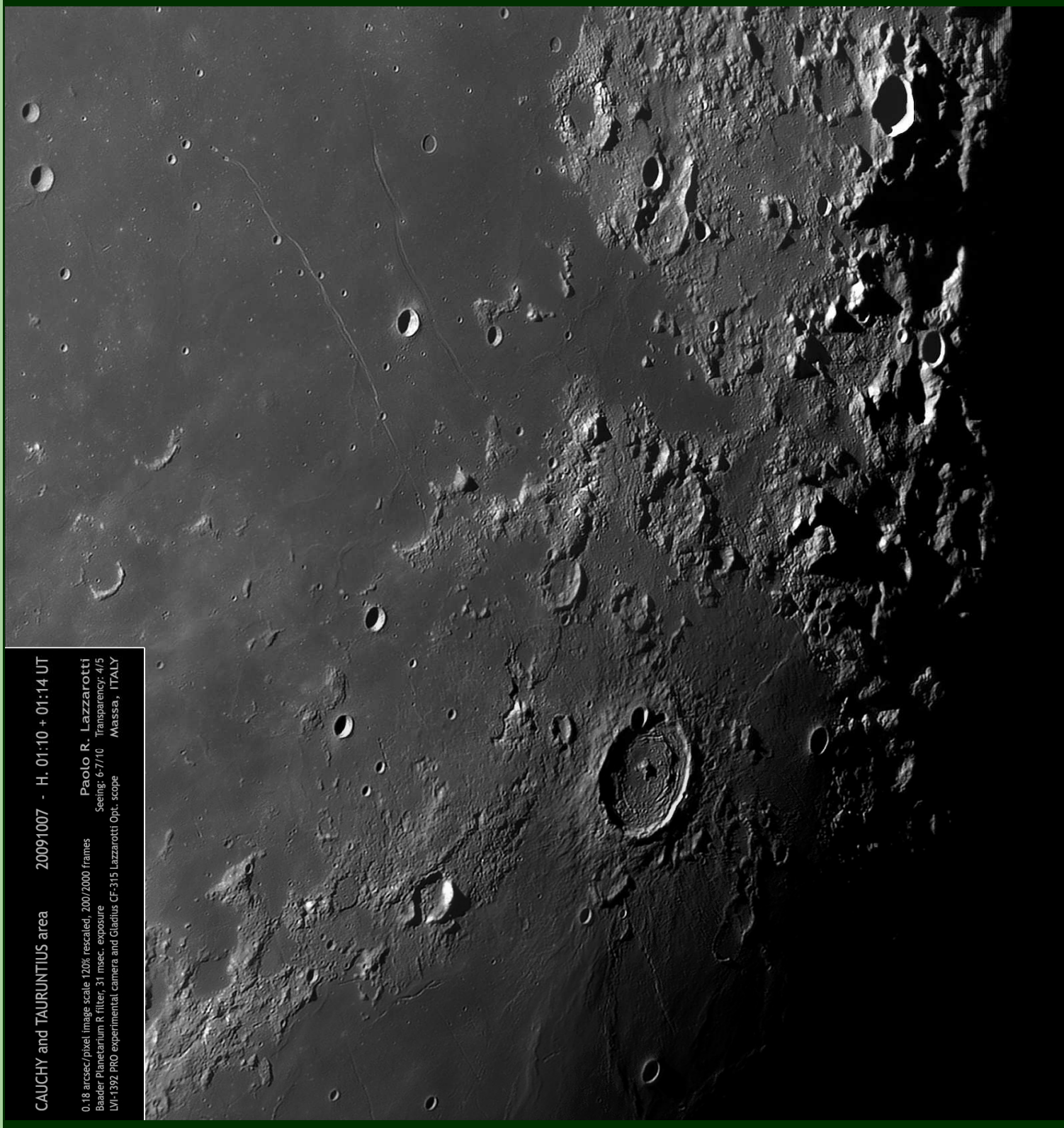

SELENOLOGY TODAY # 20

October 2010

Geological Lunar Researches Group

Selenology Today **is devoted to the publication of contributions in the field of lunar studies. Manuscripts reporting the results of new research concerning the astronomy, geology, physics, chemistry and other scientific aspects of Earth's Moon are welcome.**

Selenology Today **publishes papers devoted exclusively to the Moon. Reviews, historical papers and manuscripts describing observing or spacecraft instrumentation are considered.**

The Selenology Today

Editorial Office

selenology_today@christian-woehler.de

Cover

Paolo Lazzarotti

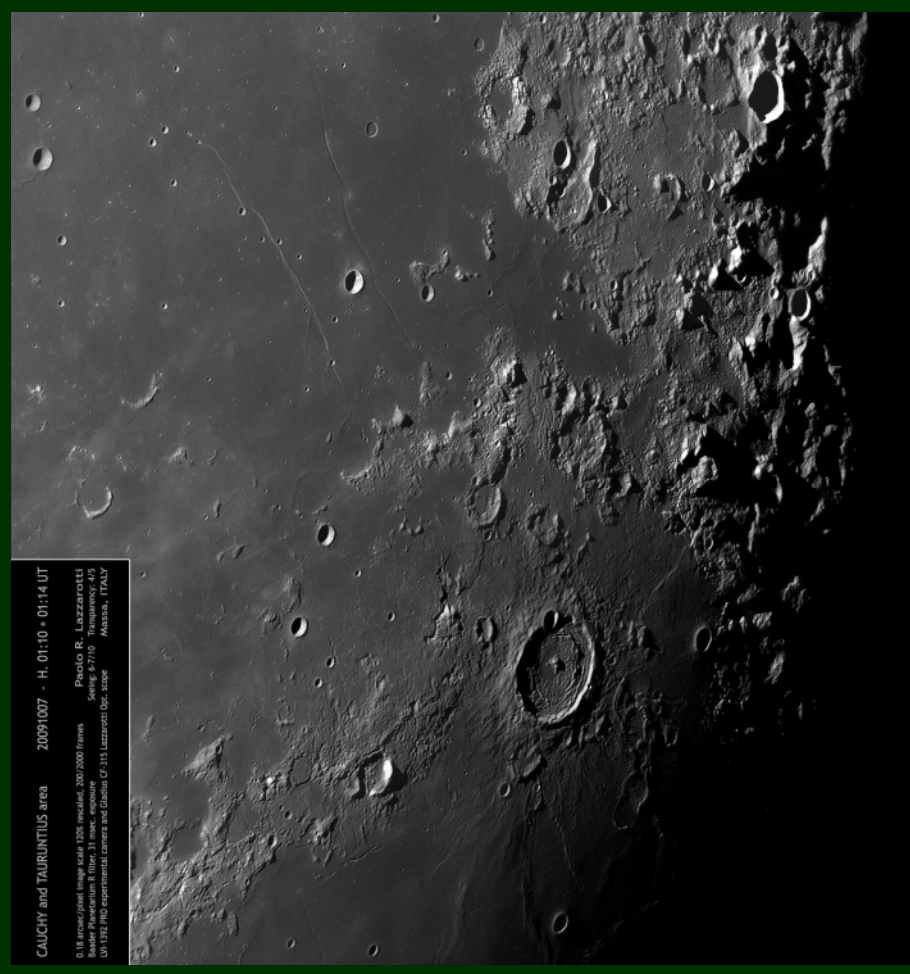

SELENOLOGY TODAY #20

Selenology Today website
http://digilander.libero.it/glrgroup/

Impressions from the Lunar Morphology Conference at Stellafane August 5, 2010 Hartness House Inn, Springfield VT

By R. Evans 1

Pitatus Rim and Crater Measurements

By H. Eskildsen 9

Arago region: composition and stratigraphy

By R. Lena.....17

Spectral Study of the Eimmart Region

by R. Evans, R. Lena, M. Clark and C. Wöhler.....37

Searching for lunar dome candidates using LTVT

by M. Collins.....61

Focus On: measuring the elevation of the Plato's craterlets

by R. Barzacchi and R. Lena.....68

Impressions from the Lunar Morphology Conference at Stellafane

August 5, 2010 Hartness House Inn, Springfield VT

By Rick Evans

Geologic Lunar Research (GLR) Group

This was my first trip to Springfield Vermont, site of the famous Stellafane amateur telescope makers convention which has been held there annually for the last seventy-five years. This year Stellafane was preceeded by a one day workshop on Lunar Morphology held at Hartness House Inn on August 5th. The workshop was organized by John Briggs and Dan Lorraine. One focus of the workshop was the history of lunar astronomy with an emphasis on the historical report by Nikolai A. Kozyrev in 1958 of spectra that he took of a brightening in Alphonsus' central peak. The workshop also addressed the concept of "reading" the moon from the stratigraphic point of view, new software tools available to lunar amateur astronomers, lunar rock and mineral mapping, a discussion of Ina crater in the context of antipodal lunar trauma caused by the SPA Basin impact, and a discussion of the LCROSS impact. I (back left in Fig.1) was one of seven invited speakers present at the workshop with the other speakers being Charles A. Wood (front left), Peter H. Schultz (front middle), Thomas A. Dobbins (back right), William P. Sheehan (front right), Ronald E. Doel (back middle) and Bert Willard (shown in Figures 6 and 7). The audience consisted of about fifty lunar enthusiasts with backgrounds that included geology, engineering, telescope making, and teaching.

Hartness House Inn

James Hartness was a former governor of Vermont and an engineer by training. He was a serious amateur astronomer and had a very ambitious equatorial turret telescope built on the grounds of his home in Springfield Vermont. His home, a large Victorian style mansion, has since become the Hartness House Inn. Hartness was a friend of Russel Porter, sometimes regarded as the father of amateur astronomy (and a co-designer of the 200 inch Hale telescope at Palomar). The exterior and interior of Hartness House is shown in the following figures. The turret telescope on the grounds of Hartness House is

a most unusual design and reminded me of a sort of World War I era cement bunker with a sort of artillery piece projecting from it (see below). To reinforce this impression, the telescope is accessed by a series of long, dark and twisting underground tunnels. Workrooms off of these underground passages have been converted into the Hartness-Porter Amateur Telescope Making Museum which is maintained by Bert Willard of the Springfield Amateur Telescope Makers.

Figure 1. Image by Ken Spencer (kenspencer@verizon.net)

Figure 2

Figure 3

Figure 4

Figures 5 and 6

Figure 7

The photos above show the Hartness telescope which is a refractor with a 10 inch Brashear objective lens. The long dark subterranean access corridors, an inside view of the telescope turret, and the museum made from one of the subterranean workshops are also shown. Bert Willard is shown in the red shirt next to the famous Porter garden telescope and at the turret telescope.

The Workshop

The conference opened with a discussion of James Hartness and Russell Porter by Bert Willard who manages the Hartness-Porter Amateur Telescope Making Museum. His lecture was titled "Russell Porter and the Moon." This was followed by two lectures by Chuck Wood, the eminent lunar scientist and stratigrapher who is perhaps best known to amateur astronomers for his column in Sky and Telescope magazine and the LPOD (Lunar Photo of the Day). The first was a guided tour of his Lunar 100, which is the lunar feature version of the Messier catalog of deep sky objects. Chuck discussed about

20 or 30 examples from his Lunar 100 series in some detail (Fig. 8). His second lecture was titled "Lunar Exploration Tools" and was a detailed description of software available to amateur astronomers to expand their studies of the moon. Examples covered during this lecture were LTVT written by Jim Mosher, the Virtual Moon Atlas (VMA) by Christian Legrand and Patrick Chevalley, the Moon Zoo, John Moore's Moon Atlas, various iPhone Apps useful to amateur astronomers, the LPOD site, MoonWiki, MoonWorld, and a research based game program under development to allow students to "build" a moon by collision.

The next lecture was by Peter Schultz, a professor at Brown University in the Geological Sciences Department who is an eminent lunar scientist who had a principal role in the recent LCROSS lunar mission (Fig. 9). His lecture was titled "Why the Two Faced Moon" and was a fascinating discussion of a theory concentrating on proposed antipodal lunar trauma caused by an oblique impact that created the SPA Basin. This trauma was proposed as causing a large number of arcuate rilles and faults surrounding Oceanus Procellarum and were termed the Oceanus Procellarum System. It was proposed that this trauma could result in outgassing from several sites, the most recent of which appears to be Ina crater which might be only 2 million years old. Ina might show the lunar surface with the regolith "blown away" by ongoing outgassing. He urged lunar amateurs to conduct a systematic study of Ina to determine if any outgassing events might be visualized as transient lunar phenomena.

Figure 8

Figure 9

Next came a series of inter-related lunar historical lectures by the well known lunar author Thomas A. Dobbins, a contributing editor to Sky and Telescope magazine (who is especially appreciated for his acclaimed book *Epic Moon: A History of Lunar Exploration in the Age of the Telescope* co-authored with William Sheehan); William P. Sheehan who is a psychiatrist by profession but with a longstanding interest in amateur astronomy and the history of astronomy (he is also a contributing editor to Sky and Telescope magazine); and Ronald E. Doel who is an Associate Professor of history at Florida State University and the author of *Solar System Astronomy in America*. William Sheehan concentrated on the work done on lunar cratering by the noted New Zealand astronomer A.C. Gifford, but within a broad historical context. Thomas Dobbins and Ronald Doel concentrated on the famous TLP event reported and spectrally analyzed by Nikolai A. Kozyrev in 1958. Dobbins pointed out controversy surrounding the data and the broader historical context of Kuiper's involvement in trying to determine the credibility of the report. It was at least my impression after listening to these lectures, that no final conclusions could be reached, but the discussion was very thorough and very interesting.

Ronald Doel's talk was followed by an automated slide presentation prepared by Raffaello Lena, editor in chief of the journal *Selenology Today* and leader of the Geological Lunar Research group (GLR). This presentation demonstrated the wide variety of lunar work conducted by GLR, and emphasized the work that the group has done in lunar dome research and particularly in the area of lunar dome classification. He also emphasized the contribution that *Selenology Today* is making to lunar studies. This lecture was very well received by the audience. This presentation was followed by my lecture titled Lunar rock and mineral mapping using public-domain software with Clementine and Lunar Prospector data: The Geological Lunar Research Group (GLR) Experience. This lecture was basically a summarization of material presented in the GLR Spectral Manual which is presented in issue No. 19 of the on-line journal *Selenology Today*. The lecture discussed working with lunar spectra from small telescopes and from the Clementine, Selene, and Lunar Prospector lunar probes. It emphasized how Clementine and Lunar Prospector spectra could be used to create rock and mineral maps of the lunar surface. Software developed by GLR was provided to interested conference participants to allow them to reproduce work that GLR has done in this area and to create their own rock and mineral maps of the lunar surface. It was emphasized that this technical ability arose from a group effort within GLR.

A lively panel discussion ensued in which conference participants probed more deeply into each of the topics covered in the morning and afternoon sessions. There was also much discussion of the future of lunar exploration. The topic gradually turned to amateur astronomy in general and its likely future evolution. Much of this centered on ways to get the next generation interested in astronomy and it appeared that astronomy club involvement was likely a key factor. There was also praise for the quality of modern equipment available to amateur astronomers and appreciation for magazine publications that make current topics in astronomy intelligible to amateurs. Following a hearty and congenial banquet, the final lecture, a fascinating summary of the LCROSS mission, was given by Peter Schultz. We learned that the LCROSS impact site was shifted from Cabeus A to Cabeus proper because it was suspected to have the highest hydrogen concentration in that area. Also, shadow cast by a large hill on the Cabeus ridge provided excellent contrast against which to view a vapor cloud post-impact. It was particularly interesting that the Centaur upper stage rocket impactor was essentially a hollow-point projectile and Schultz had observed via experimental impact modelling, that such a projectile was likely to produce a particularly high ejecta plume. Schultz concluded by saying that a detailed summary of the mission would soon appear in print when peer review was concluded.

Pitatus Rim and Crater Measurements

By Howard Eskildsen

Association of Lunar and Planetary Observers, American Lunar Society, Alachua Astronomy Club

Abstract

Images were obtained on 2010 June 05, 09:46 UT and the Lunar Terminator Visualization Tool (LTVT) was used to measure relative rim to floor and central peak to floor elevations. Under setting Sun conditions sections of the northwest rim measured 780, 490 and 430 meters ± 30 meters, a massif on the west rim 1010 meters, and the central peak 660 meters. The crater diameter measured 100 km.

Introduction

Pitatus (Fig. 1) lies on the southern margin of Mare Nubium adjacent to the smaller crater Hesiodus and is considered to be Nectarian in age, 3.92 - 3.85 billion years (Legrand and Chevalley, 2008). It has a heavily-modified rim and an off-center central peak. Its floor has been fractured and elevated and a concentric rill system encircles the margins of the floor. A narrow cleft in its western rim connects it with the adjacent crater, Hesiodus. My interest in Pitatus arose from the cleft between it and Hesiodus that produces a curious cone of light effect across the floor of the latter at lunar sunrise (Fig. 2). The measurements in this paper are intended as the first of many to better understand the nature and relations of Pitatus and Hesiodus.

Method

The image used for elevation measurements was taken from Ocala, Florida, 82.13° west, 29.18° north, with an Orion ED 80mm, 600 ml focal length refractor with 5X Meade TeleXtender, DMK 41AU02.AS, and IR-block filter. A sixty second AVI file was acquired with IC Capture.AS 2.1 and aligned and stacked with Registax 4 to produce a single image. Further processing was done with Photoshop Elements 6.0 to sharpen and adjust tones and contrast of the image. The image was calibrated with the Lunar Terminator Visualization Tool (LTVT) using craters Guericke B and Wilhelm D, which were located on opposite corners of the original image, as reference craters. Guericke B is on the ULCN 1994 list of control points, but I discovered later that Wilhelm D is not, so I used the “identify nearest named feature” mouse option to locate the positions of

Pitatus, Hesiodus, Hesiodus A, and Gauricus on the calibrated photograph. The program placed identification marks very nearly dead center on all four craters, so I believe the calibration is quite accurate. The reverse shadow length mode was used to determine the relative elevations of the features measured. The reference point, marked by a blue "+" symbol, was carefully placed at the margin of the shadow and then the cursor was placed as precisely as possible over the intersection of the shadow margin and the red line that radiates sunward from the reference point.

Estimated elevation and the lunar coordinates of the point of measurement were recorded from the LTVT data box. After carefully recording coordinates and measurements listed in this paper, the measurements were then repeated several times and the greatest difference from the original readings were used to estimate the measurement error.

Results

Pitatus crater diameter (Fig. 3): 100 km

It is interesting to note that the central peak lies 10 km from the center of the crater at an azimuth of 290°. Elevation measurements are shown with error estimated at ±30 meters (Fig. 4).

Discussion

Comparison of diameter listed by Pike,100 km (Pike,1976), and NASA Catalog of Lunar Nomenclature, 97 km (Anderson and Whitaker 1982) shows the result above to be within 3% of their measurements. The central peak elevation of 660 meters is considerably lower than the 1000 meter height measured by Sekiguchi (Wood, 2010) but higher than the 500 meters listed in Wikipedia (Author not listed, 2009). Multiple measurements would help refine the measurement and settle concerns about any possible slope to the crater floor. The three northwestern rim measurements are consistent with rim height of 680 meters measured by Pike (Pike, 1976), and suggest a down sloping of that section from the northern portion to the southern end. This agrees with its general appearance on the photo. Measurements of the southeastern rim were not possible due to its severe modification and erosion from later impacts. The 1010m prominence on the west rim arbitrarily labeled "west massif," probably represents material thrust up by the impacts of both craters and may be the highest point in the region.

Conclusion

Measurements of crater dimensions of highly modified craters such as Pitatus are possible with small telescopes, but are problematic and require multiple measurements to adequately define its contours. The error margin for the elevations represents the precision of the measurements, but additional measurements might be necessary to establish the true accuracy. Higher resolution photos with larger apertures would greatly improve the accuracy and multiple images under varying light conditions would further elucidate its dimensions.

References

[1] Anderson, L., Whitaker, E., 1982. NASA Catalogue of Lunar Nomenclature, NASA Reference Publication 1097, p 57.

[2] Author not listed, 2009. Pitatus (crater), Wikipedia, URL: http://en.wikipedia.org/wiki/Pitatus_(crater), (last date accessed, 23 June 2010).

[3] Pike,R., Menlo Park, 1976. Crater Dimensions from Apollo Data and Supplemental Sources, US Geological Survey, p464.

[4] Legrand, C., Chevalley, P., 2008. Virtual Moon Atlas Exepert 3.5c

[5] Wood, C., 2010. Lunar Photo of the Day, June 9, URL: http://lpod.wikispaces.com/June+9,+2010, (last date accessed, 23 June 2010).

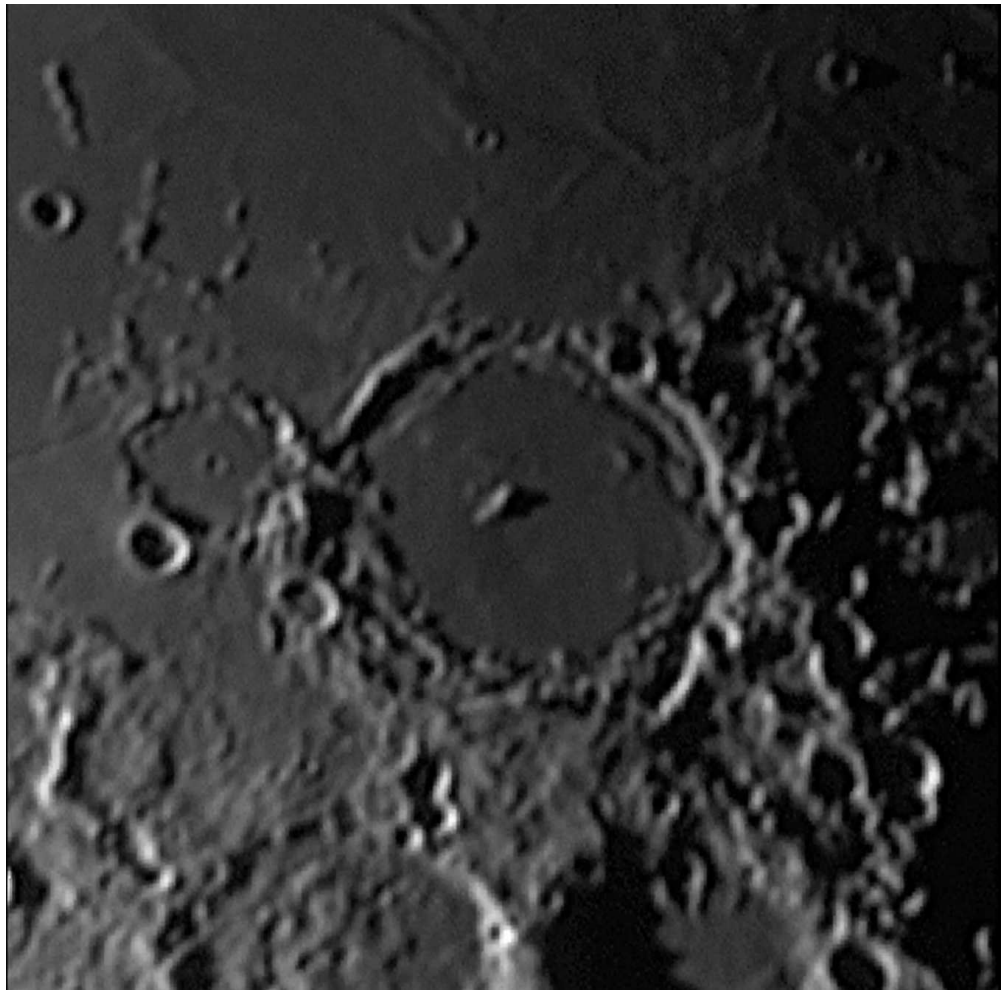

Figure 1

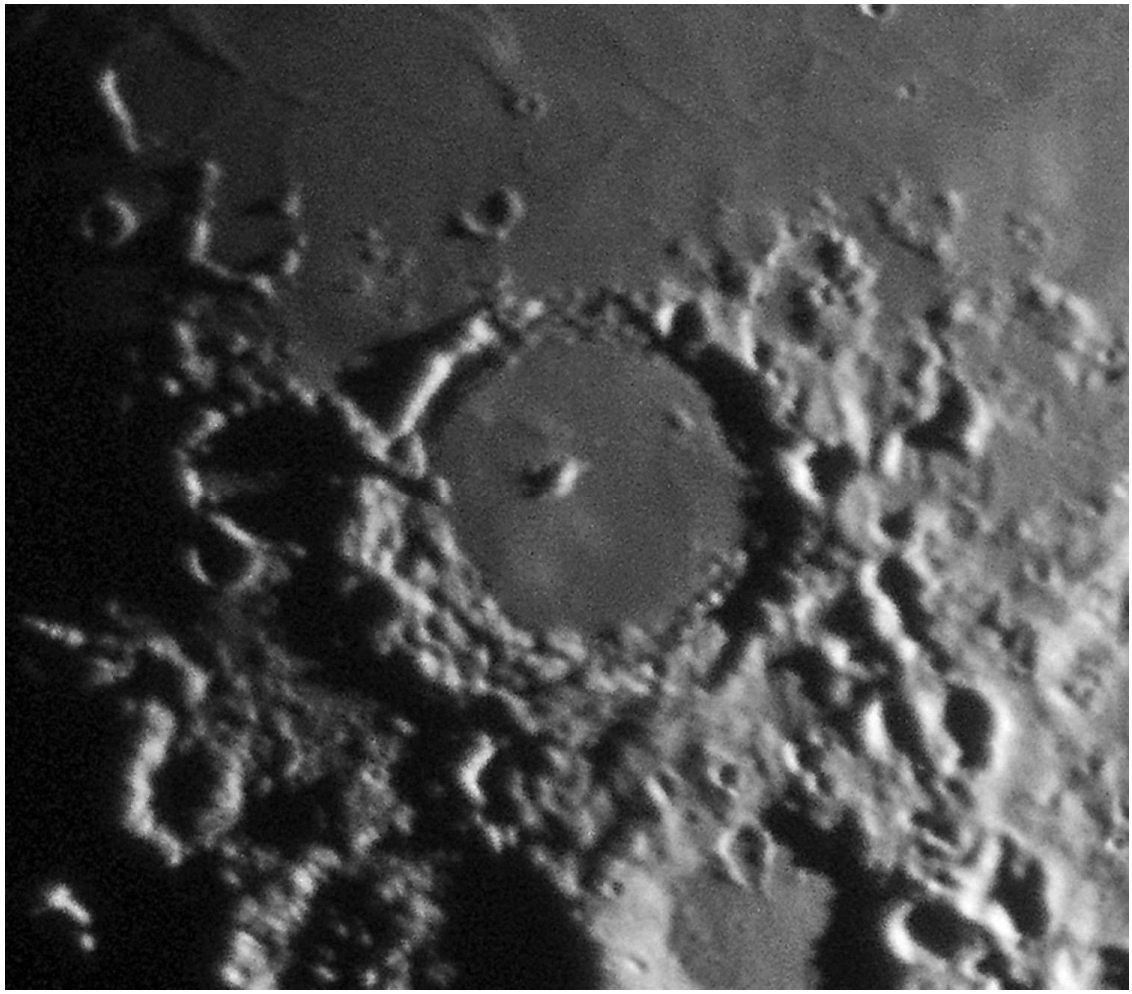

Figure 2

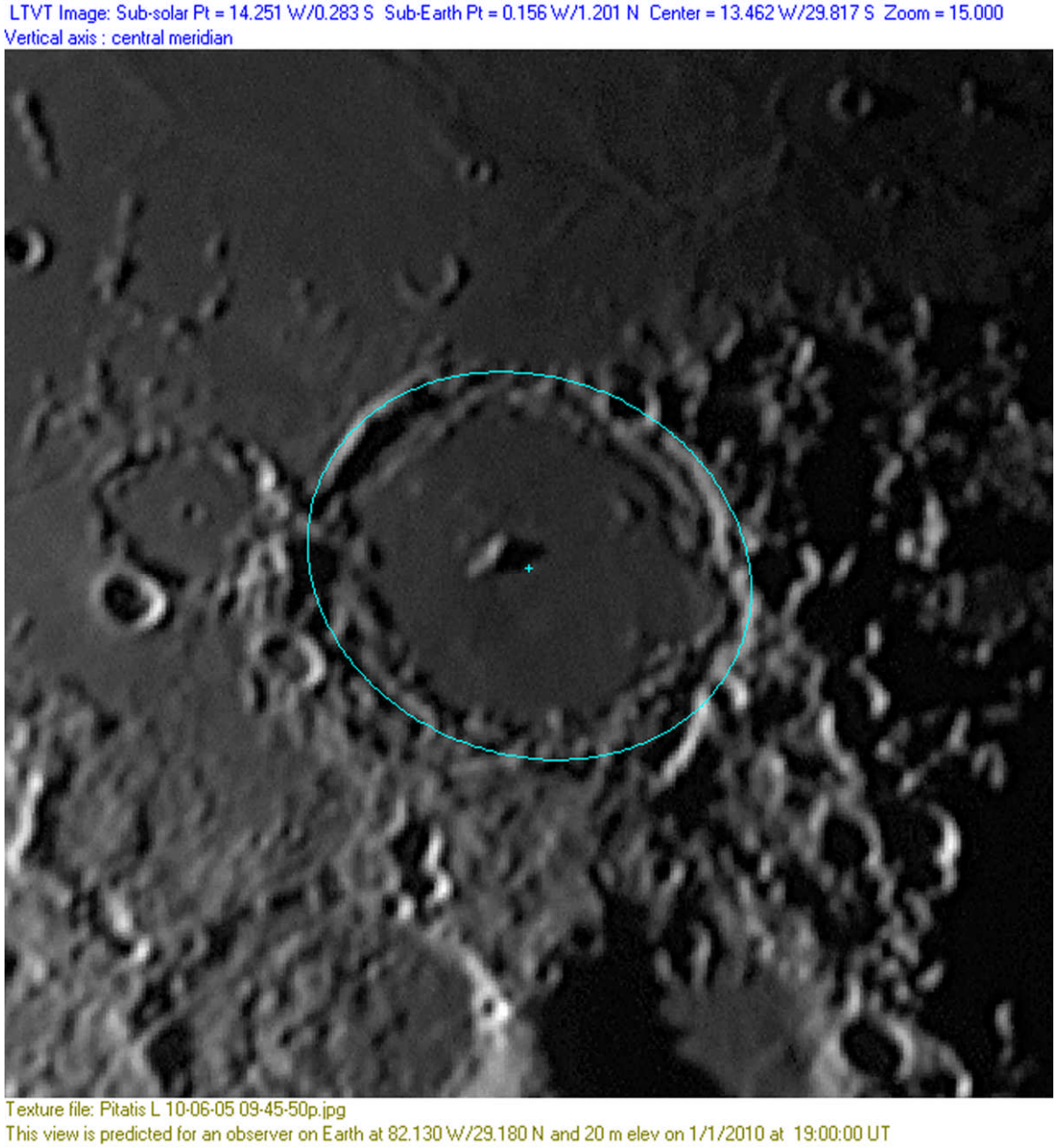
LTVT Image: Sub-solar Pt = 14.251 W/0.283 S Sub-Earth Pt = 0.156 W/1.201 N Center = 13.462 W/29.817 S Zoom = 15.000
Vertical axis : central meridian
Texture file: Pitatis L 10-06-05 09-45-50p.jpg
This view is predicted for an observer on Earth at 82.130 W/29.180 N and 20 m elev on 1/1/2010 at 19:00:00 UT

Figure 3

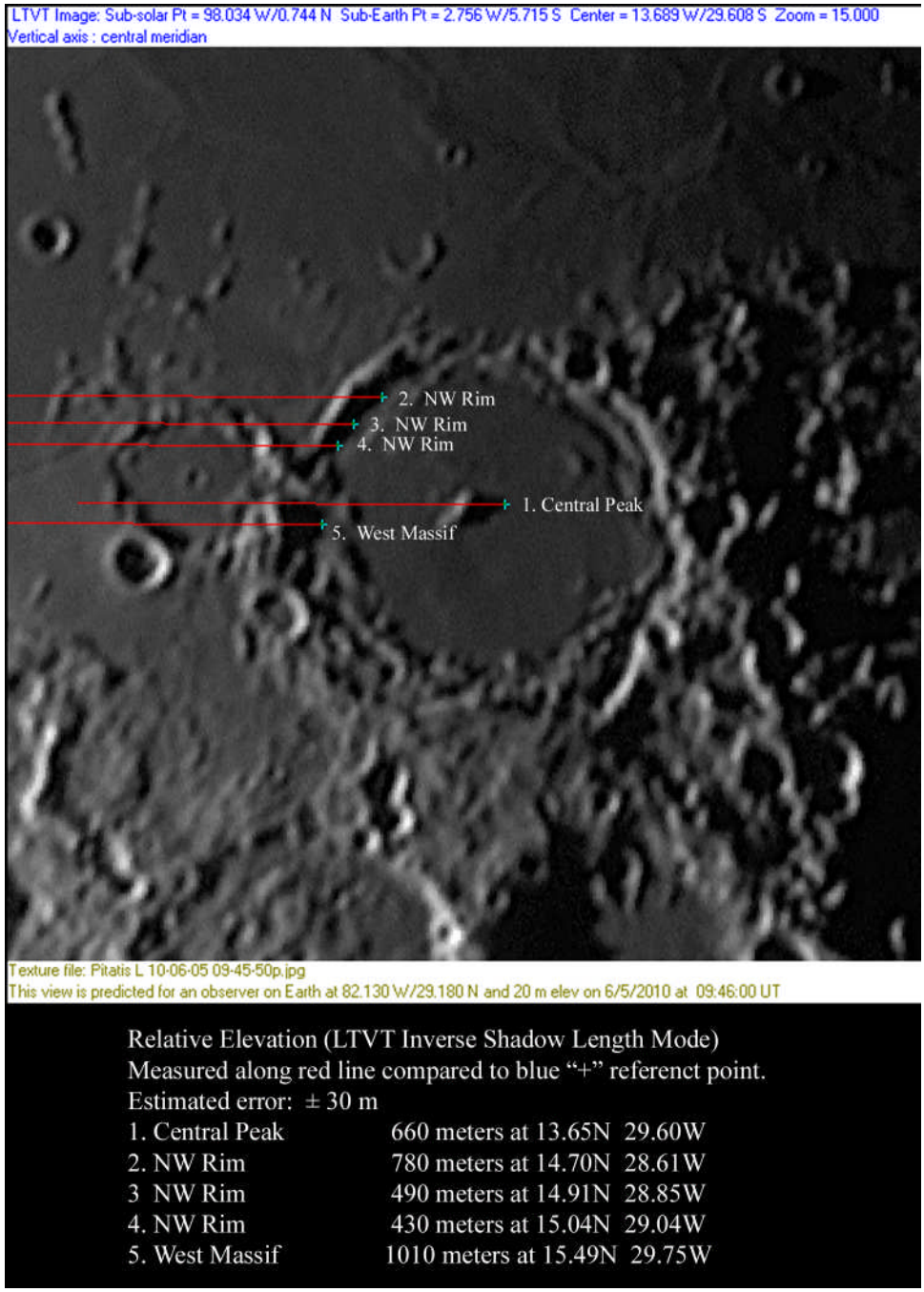
LTVT Image: Sub-solar Pt = 98.034 W/0.744 N Sub-Earth Pt = 2.756 W/5.715 S Center = 13.689 W/29.608 S Zoom = 15.000
Vertical axis : central meridian
2. NW Rim
3. NW Rim
4. NW Rim
1. Central Peak
5. West Massif
Texture file: Pitatis L 10-06-05 09-45-50p.jpg
This view is predicted for an observer on Earth at 82.130 W/29.180 N and 20 m elev on 6/5/2010 at 09:46:00 UT
Relative Elevation (LTVT Inverse Shadow Length Mode)
Measured along red line compared to blue "+" referenct point.
Estimated error: ± 30 m
1. Central Peak 660 meters at 13.65N 29.60W
2. NW Rim 780 meters at 14.70N 28.61W
3 NW Rim 490 meters at 14.91N 28.85W
4. NW Rim 430 meters at 15.04N 29.04W
5. West Massif 1010 meters at 15.49N 29.75W

Figure 4

Table 1

Feature	Elevation	Lunar Coordinates
1. Central Peak	660 meters	13.65N 29.60W
2. NW Rim	780 meters	14.70N 28.61W
3 NW Rim	490 meters	14.91N 28.85W
4. NW Rim	430 meters	15.04N 29.04W
5. West Massif	1010 meters	15.49N 29.75W

Arago region: composition and stratigraphy

By Raffaello Lena

Geologic Lunar Research (GLR) group

Abstract

This study uses a spectral mapping technique based on Clementine UVVIS-NIR imagery to assess the composition and stratigraphy of Mare Tranquillitatis and crater Arago. Elemental abundance maps for Al, Ca, Fe, Ti, O, and Mg were generated using a matrix regression based spatial enhancement of Lunar Prospector data. In this work a petrographic basalt map is introduced. The goal was to evaluate the composition of the mare soil around Arago and the domes Arago α and β. The Arago floor exhibits spectral properties characteristic of non mare feldspathic materials. The walls and the central mountains of the crater show spectral properties characteristic of mare material characterized by titanium rich basalt. The spectral character of the Arago ejecta is attributed to the excavation of underlying and less titanium-rich Th basalts and non mare feldspathic material, confirming that the Th unit is stratigraphically older than the overlying Tvh-A basalts.

According to the spectral map and the basalt map also Arago D and several small craters that occur within these deposits exhibit a distinct "blue halo" excavating Ti-rich mare basalt up to the surface. These small craters are interpreted to have re-exposed the Tvh-A surface basalts from just below Arago's ejecta deposit. The corresponding petrographic maps indicate that the soil around the domes Arago α and β appears composed of highland-like material mixed with mare basalt. The highland contamination in the mare soil is more pronounced to the north than to the west, where the dome Arago β is localized. The soil around two domes displays similar elemental composition because of mixing between basalts and highland material.

1.Introduction

As reported by Rajmon and Spudis (2001), the older lavas in Mare Tranquillitatis are characterized by a lower Titanium content (reddish in colour ratio), while the youngest

lavas erupted in the region have a higher Titanium content (blue in colour ratio). The units richest in TiO_2 are denoted Tvh-A and the Tvh-B by Staid et al. (1996).

Both the Tvh units appear to be spatially continuous and are only interrupted by patches of less blue basalts and impact crater ejecta. Another mare unit (Th) is mapped by intermediate fractions of the red and blue mare end-members and occurs as small patches within the two bluer units. These discontinuous less blue basalts are interpreted to have lower (but still relatively high) titanium abundance and are designated as the Th (high titanium) unit. A fourth basalt unit (Tl) occurs in the north eastern and south eastern corner of Tranquillitatis and is interpreted to have low-titanium contents (Staid et al., 1996). These Tl basalts are spectrally similar to the low-titanium Serenitatis basalts (MS2) but are much more heterogeneous (cf. Fig.1).

False color image made using Clementine imagery shows color differences of individual units within the mare (Staid et al., 1996, and references therein). The Tvh-A basalt unit extends from the north western part of Tranquillitatis around the western side of the Lamont and as far south as the Apollo 11 landing site in south western Tranquillitatis. An extensive spectrally blue Tvh-B unit extends in the north, south, and central eastern portions of the basin.

The red Tl basalt unit occurs in the north eastern and south eastern corner of Tranquillitatis. However high contrasts between mare basalt and highland substrate allows identification of craters that have penetrated mare basalt, which has implication in stratigraphy. Distribution of Mare Tranquillitatis basalts with various titanium content are reported in previous works (Pieters, 1978; Wilhelms, 1987; Hiesinger et al., 2000; Hiesinger et al. 2001).

Most domes in Mare Tranquillitatis are formed out of the same lava as observed around them and are thus spectrally indistinguishable from their surrounding.

The well known domes termed Arago α and β (Fig. 2b) have relatively gentle slopes (1.5° and 1.3°), large diameters (>20 km), and high volumes (>30 km). Likely they formed over a long period of time, compared to the other domes in that region, during which the lava poured out more or less continuously, forming a high volume edifice, as described in previous studies (Wöhler et al., 2006; Lena et al., 2005). This is supported by their morphology with complex surface detail, implying a variety of individual flow units.

Arago α is spectrally redder than its surrounding mare soil. A similar relation can be

observed for domes Cauchy τ and ω, but there the outline of the spectrally bluer Tvh-B lava layer is more irregular.

This study aims for determining the elemental, mineralogical, and spectral characteristics of the geologic units of Mare Tranquillitatis and around Arago crater using Clementine UVVIS+NIR data.

The results are compared to previous work introducing the use of a "petrographic basalt" mapping technique for stratigraphic studies of lunar features of interest.

2. Spectral analysis of the Arago region and Mare Tranquillitatis

This work employs the Clementine UVVIS+NIR spectral mapping technique developed by Evans et al. (2009a; 2009b). The technique is used to produce spectral maps of the principal spectral mafic absorption features for lunar terrain of interest. It was employed here in an attempt to discern the mineralogy of the examined region. The spectral mapping was obtained using the implementation in Octave as described by Evans and Lena (2010).

The 5 UVVIS (415, 750, 900, 950, and 1000 nm) and 4 NIR wavelengths (1100, 1250, 1500, 2000 nm) are available at the PDS Map-a-Planet site (http://www.mapaplanet.org/explorer/moon.html).

The spectral data (Fig. 3) resulted in the automated production of maps concerning:

a) band center minimum

b) band depth

c) FWHM (full height at half maximum).

Examination of spectral maps prepared using the Clementine UVVIS+NIR dataset reveals that the region of Arago is composed of admixed quantity of clinopyroxene, orthopyroxene and olivine (Fig.3). A band center minimum near 1.10 μm, is detectable to the northern mare soil. The walls of Arago, like the central mountains of the crater, are composed almost exclusively of clinopyroxene bearing rock with a band center near 0.98 μm, and a FWHM of between about 0.19 to 0.23 μm. There is no indication of the presence of orthopyroxene and olivine. In contrast, the floor of the crater is composed of

orthopyroxene, in part admixed with high-Ca pyroxene, with a band center between 0.890 to 0.950 μm. The segregated maps corresponding for orthopyroxene band center (0.890 to 0.945 μm), clinopyroxene band center (0.950 to 1.000 μm), and olivine band centers (1.005 to 1.100 μm), are used to derive a false color map where the red channel is assigned to orthopyroxene, green channel to olivine and blue channel to clinopyroxene (Fig.3).

No particularly difference is noticeable in the corresponding OMAT values between the western and northern mare soil around the Eratosthenian crater Arago (Fig. 2a).

The false color image made using Clementine imagery (R=0.750/0.415, G= 0.750/0.950, B= 0.415/0.750) shows color differences of individual units within the examined region. Basalts appear blue to orange, fresh basalts are yellow to green, highlands appear red and fresh anorthosites appear blue.

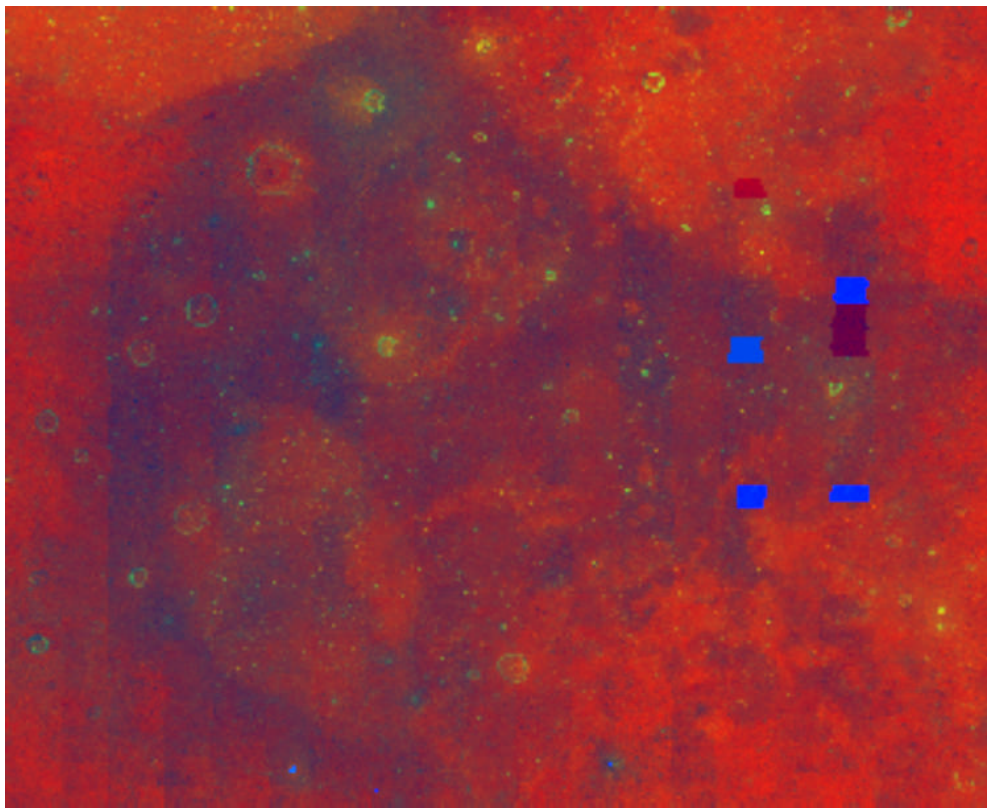

Figure 1 Mare Tranquillitatis

false color image made using Clementine imagery (R = 0.750/0.415, G = 0.750/0.950, B = 0.415/0.750). For all the images north is up and west to the left.

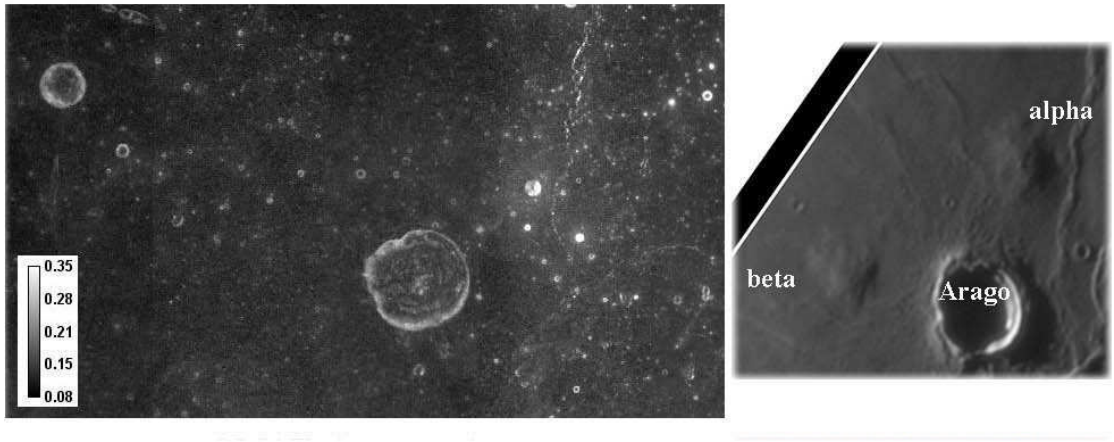

2a **2b**

Figure 2 (a) OMAT map of Arago crater and (b) the domes Arago α and Arago β.

The false color image (Fig.4) indicates regionally lower levels of titanium within and surrounding the crater Arago. A subsequent small impact crater in Arago's ejecta blanket exhibits a blue halo that spectrally matches adjacent titanium rich units (cf. Fig.4). Furthermore the dome Arago α is spectrally redder than the lavas of Arago β.

The spectra were then represented as continuum divided UVVIS+NIR spectra (Fig. 5). The continuum division by the line between the 750 nm and the 1500 nm reflectance value was not fully appropriate for the Mare Tranquillitatis region because of spurious maximum values larger than 1. Hence, for this work, a more appropriate continuum division by the line between 750 and 1250 nm was used.

The individual Clementine spectral plot for the wall and the central mountain of the crater is also consistent with the presence of high-Ca pyroxene. The floor of Arago is spectrally characterized by a shallow absorption band consistent with the presence of a low-Ca pyroxene, which is admixed with a high-Ca pyroxene. The crater Arago D, located to the east of Arago, is characterized by a broad and depth pyroxene absorption at 0.99 μm due to a high-Ca pyroxene.

The soil around the dome Arago α displays an absorption band between 0.89 to 0.95 μm with a secondary broad absorption band centred at about 1.10 μm (Fig. 5), which likely is due to the presence of an olivine component. The olivine absorption band is not present in the spectrum of the dome Arago β, demonstrating a mineralogical difference between the western and northern mare soils around the Arago crater.

3. Calculation of Elemental Abundances using Clementine UVVIS+NIR data

Lunar Prospector (LP) data provides elemental abundance ground truth, but at low spatial resolution. This resolution, however, may be increased using the method described by Wöhler et al. (2009) which represents LP data in terms of a transformation of spectral parameter maps for the absorption trough near 1.00 μm derived from Clementine UVVIS+NIR imagery. Creation of these spectral maps is discussed in Evans et al. (2009a). Mathematically, a data matrix can be represented by the transformation of a second matrix according to equation (1) where matrix x and matrix b are of the same width:

$$Ax = b \qquad (1)$$

Using this model, the global LP elemental abundance map for a given element is termed the ground truth matrix and is matrix b. It is a row matrix of height one and width equal to the row*column dimension of the LP image. A set of spectral parameter maps includes the band center, band depth, FWHM and slope, where only the deepest minimum is regarded, and their quadratic combinations. Each row in matrix x consists of one of these spectral maps written as a single row matrix of height one and width equal to the row*column dimension of the map image. In addition to the spectral maps described above, their pairwise product maps are also added to matrix x. Matrix A is the coefficient matrix giving the gain and offset values that matrix b must be applied to effect its transformation into a form approximate to matrix x.

When the equation Ax = b is solved for A using standard linear algebra techniques, one obtains the gain and offset coefficients necessary to transform matrix x into an approximation of the ground truth matrix b. Matrix A has height one and width equal to the number of rows in matrix x. The last element in Matrix A is the offset and all other elements are gain coefficients. This feature set does not comprise the albedo itself, and produces a similarly good fit to the global LP data as the Lucey Fe and Ti abundances (Lucey et al., 2000).

These gain and offset coefficients, once derived, are also applicable to any other set of Clementine based spectral maps even though they represent a much higher spatial resolution than the global maps used to determine the coefficients. The uncertainty of the derived elemental abundance maps is ± 1 wt%. Based on this approach, the abundances of the elements Ca, Al, Fe, Mg, Ti, and O were estimated (Fig. 6). The wt % range for

the Figure 6 is as follows: aluminum (0-20 wt %), calcium (2-18 wt %), iron (0-25 wt %), magnesium (0-16 wt %), oxygen (40-47 wt %), and titanium (0-6 wt %).

4. Petrographic maps

The topographic distribution of rock types can be derived from elemental abundance maps using the three end-member model described by Berezhnoy et al. (2005). The petrographic maps shown in Figures 7 and 8 indicate the relative fractions of the three end-members mare basalt (red channel), Mg-rich rock (green channel), and ferroan anorthosite (FAN, blue channel). The soil of Arago α appears composed of highland-like material admixed with mare basalt. The petrographic map also indicates regionally redder deposits around Arago (Fig.7).

Another petrographic map (Fig. 9), termed petrographic basalt map, was then represented as relative fractions of the three end-members: Red for mare basalt with low Titanium amounts (Al 9 wt%, Ti 1.5 wt%), Green for highland-like material (Al 14 wt%, Ti 0.5 wt%) and Blue for titanium rich basalt (Al 6.3 wt%, Ti 3.6 wt%). The basalt petrographic map of the Tranquillitatis basin is also shown in Fig. 10.

The basalts around Arago appear admixed by highlands material, thus the mixture of red mare basalt and blue FAN in the general petrographic map (Fig.7). In the basalt petrographic map, shown in Fig. 9, this mixture appears in green colour, as a high-Aluminum basalts (e.g. in the Mare Frigoris region) which obviously have a composition intermediate between those of normal mare basalt and highland material. However in Mare Frigoris there are not dark halo impact craters which shows that the composition of the basalt itself is anomalous and that there is no mixing of normal basalt with highland material. In contrast, near Arago there are many spectral halo craters which brought Ti-rich mare basalt (blue) up to the surface.

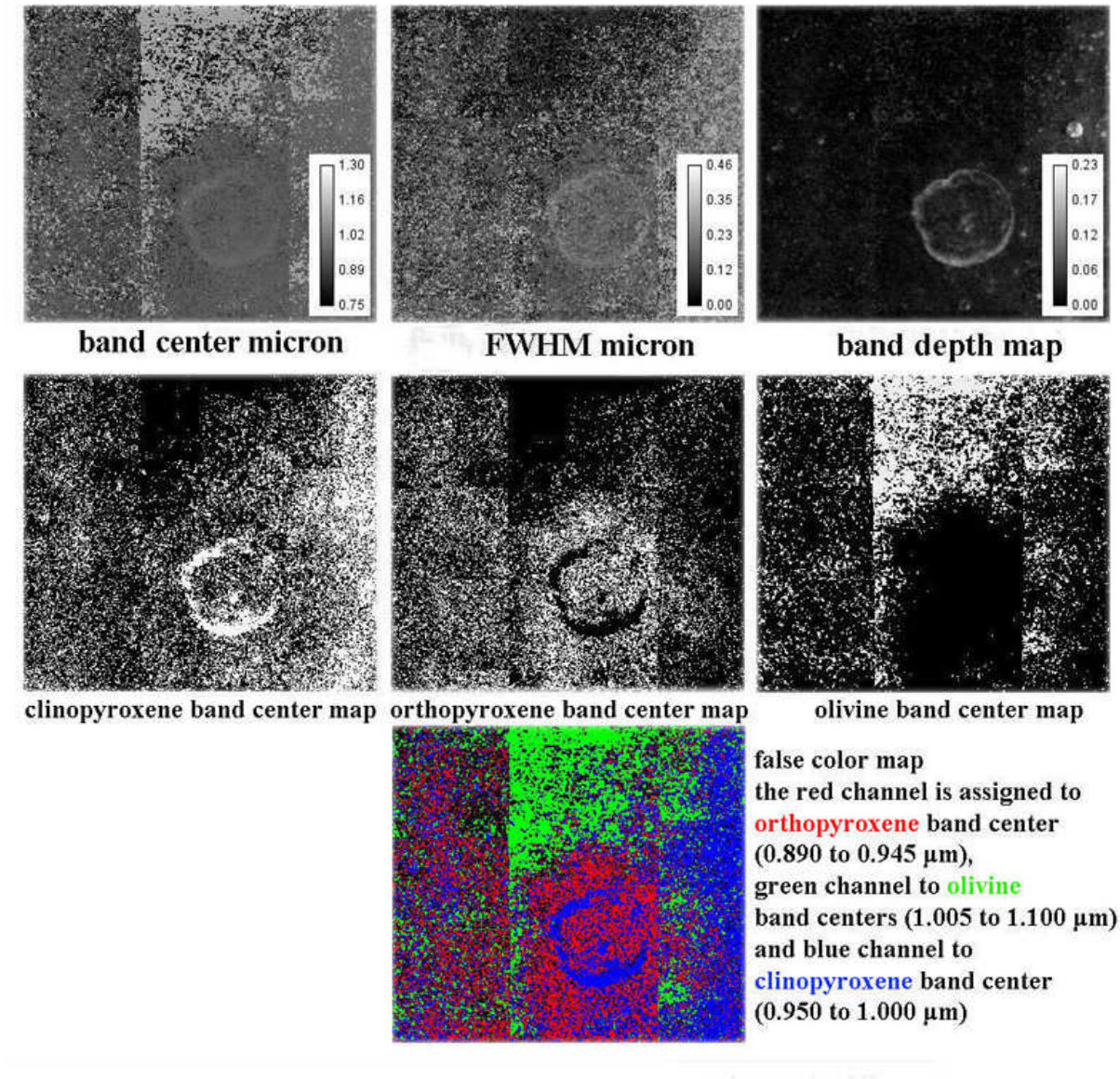

Figure 3 spectral data about Arago region

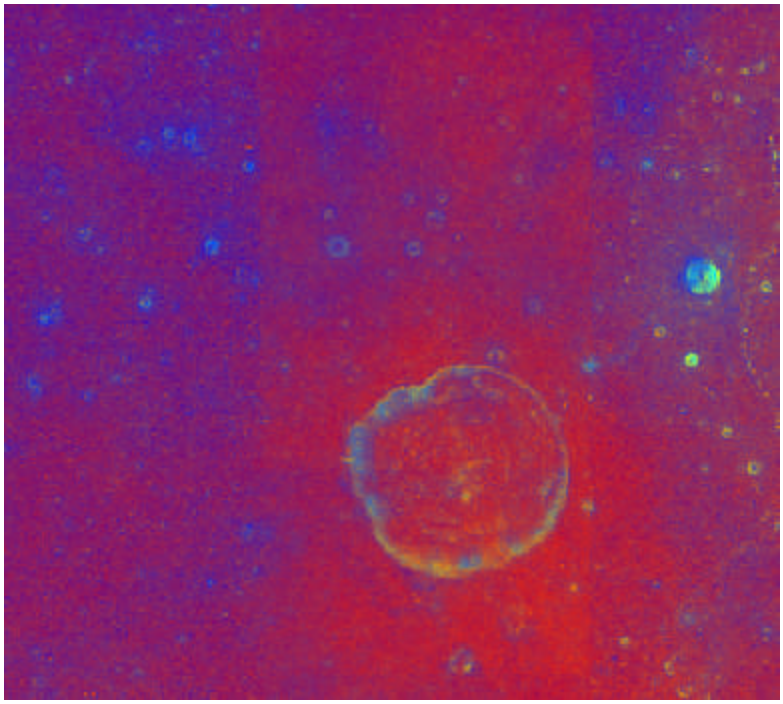

Figure 4 false color image made using Clementine imagery (R=0.750/0.415, G=0.750/0.950, B= 0.415/0.750)

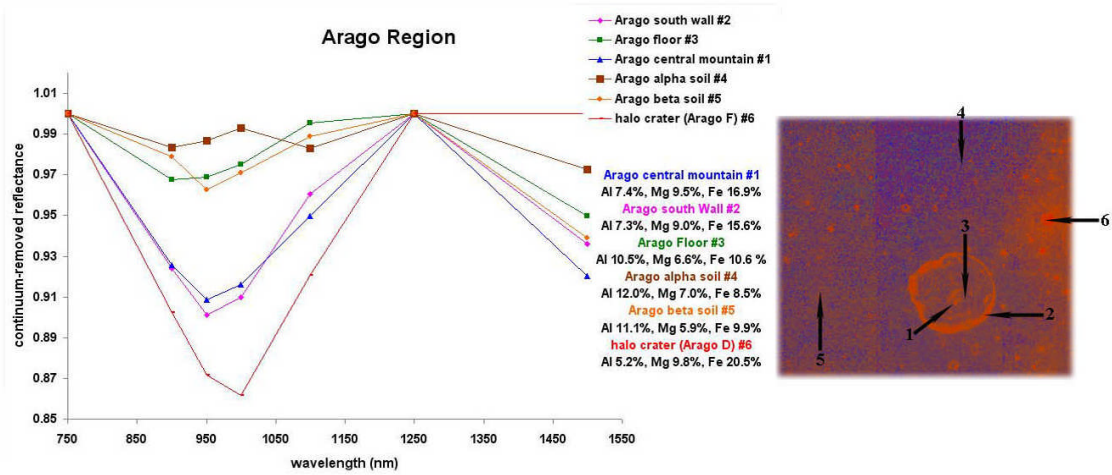

Figure 5 individual Clementine spectral plot represented as continuum divided UVVIS+NIR spectra.

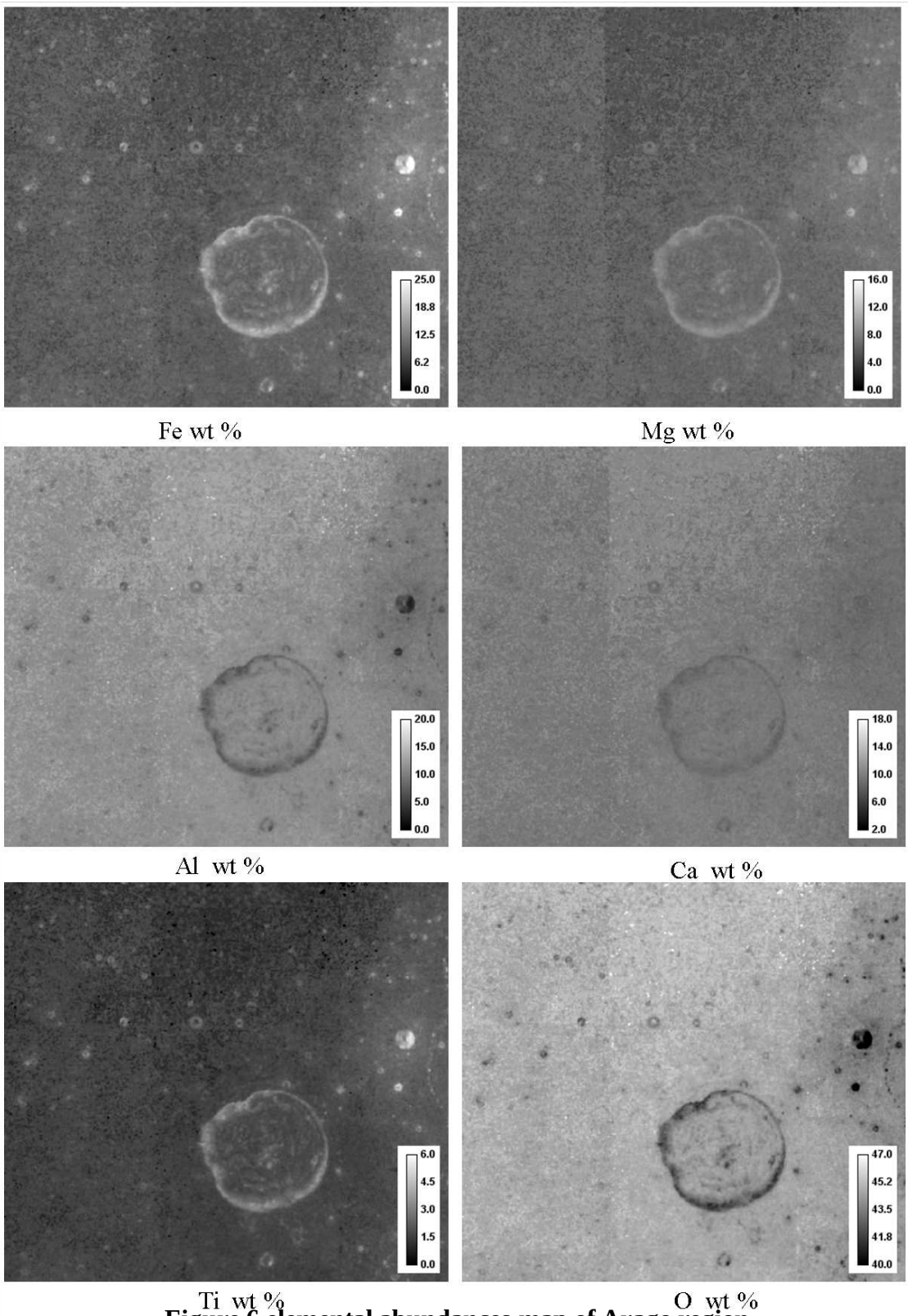

Figure 6 elemental abundances map of Arago region

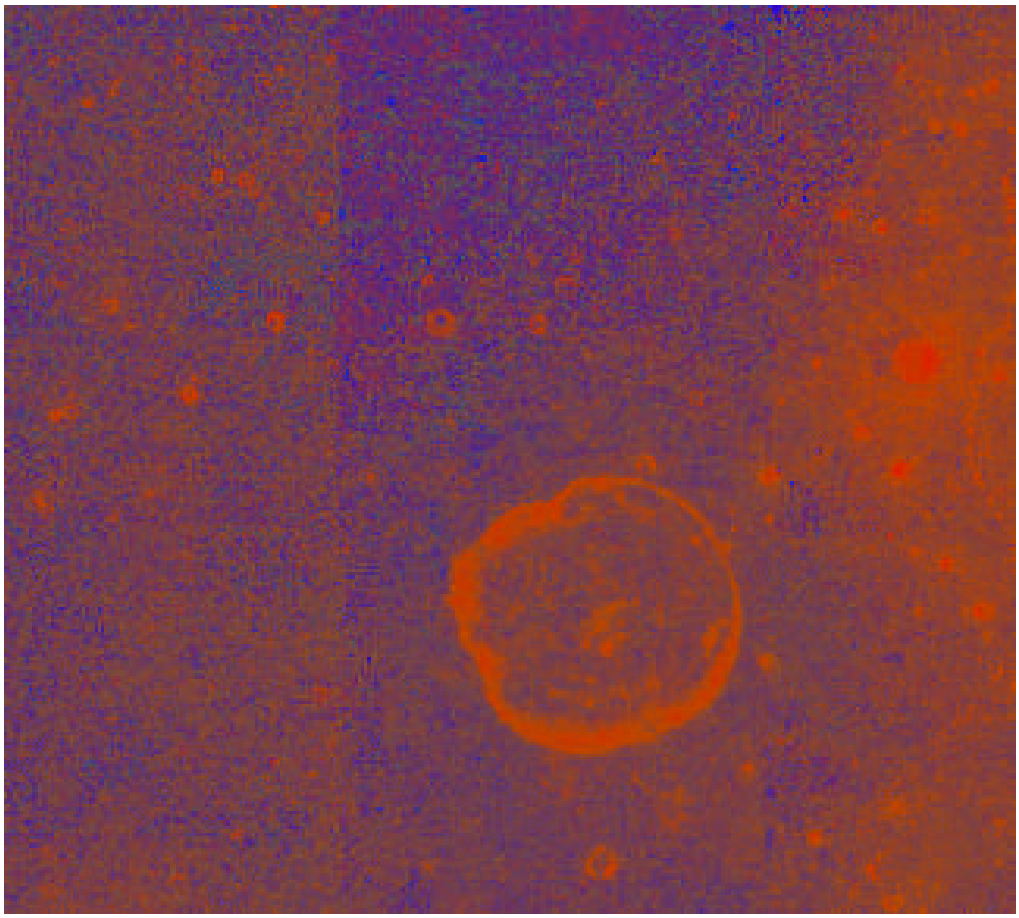

Figure 7 petrographic map of the restricted region around Arago

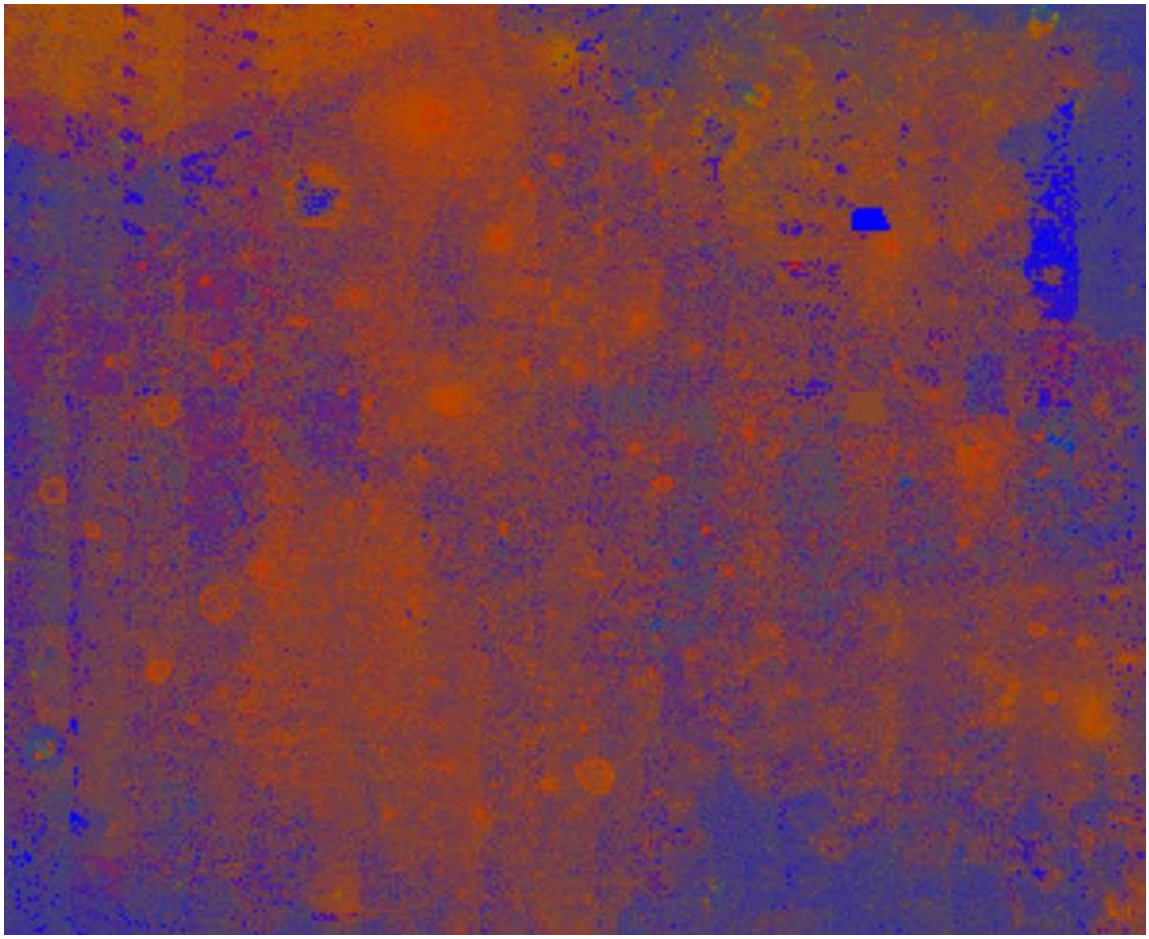

Figure 8 topographic distribution of rock types for the Tranquillitatis basin derived from elemental abundance maps (as described in the text)

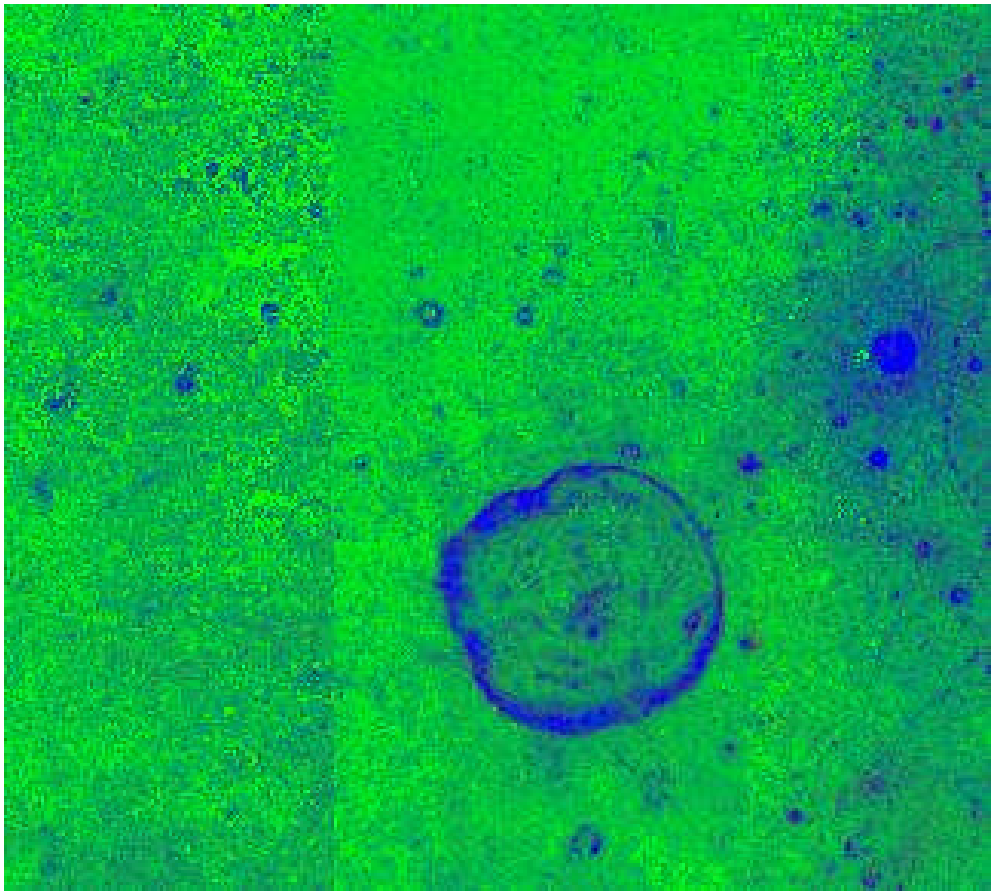

Figure 9 basalt petrographic map of the restricted region around Arago

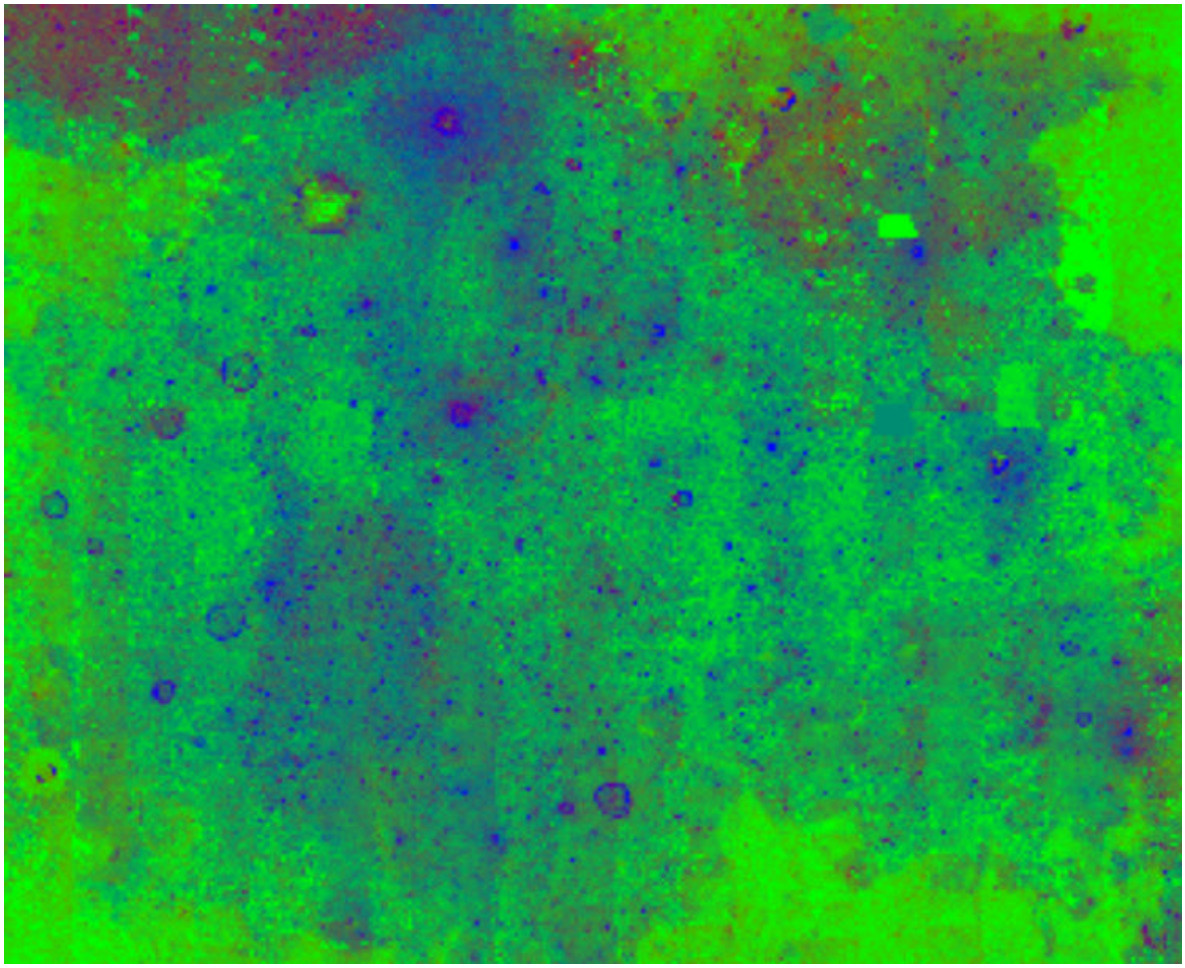

Figure 10 basalt petrographic map of the Tranquillitatis basin

5. Results and discussion

The Mare Tranquillitatis map (Fig. 11) shows a range of Fe concentration (7– 23 wt%). The iron concentration typically increases from mare margin toward center, but also varies within the mare. Iron distribution patterns in Maria Tranquillitatis is controlled by local impact excavation of iron-poor basement from beneath basalt flows (i.e., vertical mixing), but at some areas the iron distribution is mainly controlled by ejecta of large impact craters (i.e., lateral mixing). Some old craters with highland composition occur at several places throughout Mare Tranquillitatis (mainly in the east). Plinius is the most prominent example of a crater that excavated this basement and it appears dark in the Iron map of Fig. 11 and strongly green in Fig.10.

Titanium concentration in the Mare Tranquillitatis soil varies from less than 0.3 to 5 wt% Ti (Fig. 12). This variation is caused in part by highland contamination (as indicated by the iron map) and also by variation in the basalt composition. The Titanium abundances, however, vary also between units with similar levels of the contamination (Fe) and indicate the existence of several basalt types in the mare with different Ti contents. This variation in basalt composition stands out even more clearly from the basalt titanium data. Titanium content of mare soils is generally lowered by locally excavated basement material, but the relative distribution of titanium is controlled by the composition of underlying basalt and ejecta of large impact craters (Fig.12).

Regionally high abundances of the red mare end-member identified in Clementine false color map (Fig. 1) occur around the impact craters Arago, Plinius, Maclear, and Maskelyne within otherwise continuous regions of bluer mare. These impact craters appear to have excavated and re-deposited the stratigraphically older Th unit onto the younger Tvh basalts. According to previous studies (Rajmon and Spudis, 2004) volcanism in Mare Tranquillitatis started with low-Ti basalts and evolved toward medium and high-Ti basalts. However, some of the high-Ti basalts in Mare Tranquillitatis began erupting quite early, contemporaneously with the low and medium-Ti basalts, and even form the oldest units exposed on mare surface. The corresponding petrographic maps shown in Fig. 8 and 10 are also consistent with the presence of highland material which is admixed with mare basalts. In fact, the basalt petrographic map (Fig.10) shows mixing with highland material and clearly the distinction between Ti-rich (blue) and Ti-poor (red) basalt not only in the general colour but also in the colour of the material excavated by impact craters. This distinction is clear between Mare Tranquillitatis and Mare Serenitatis, but also the well-known Ti-poor basalt deposit in north eastern Mare Tranquillitatis is well visible, leading to impact craters with red-orange halos in the Ti-poor deposit in contrast to impact craters with bluish halos in the larger Ti-rich regions.

Indication of such stratigraphy is clearly visible in the Lamont area, where small craters appeared to excavate high-Ti basalt from beneath medium-Ti basalt (Figs. 1 and 10). On the contrary Dawes, Vitruvius and Carrel appear to have excavated low-Ti basalt (Ti 1.5 wt %).

Therefore, according with Rajmon and Spudis (2004), the upper part of the stratigraphic column of basalts in Mare Tranquillitatis must consist of overlapping flows with alternating medium to high TiO_2 contents.

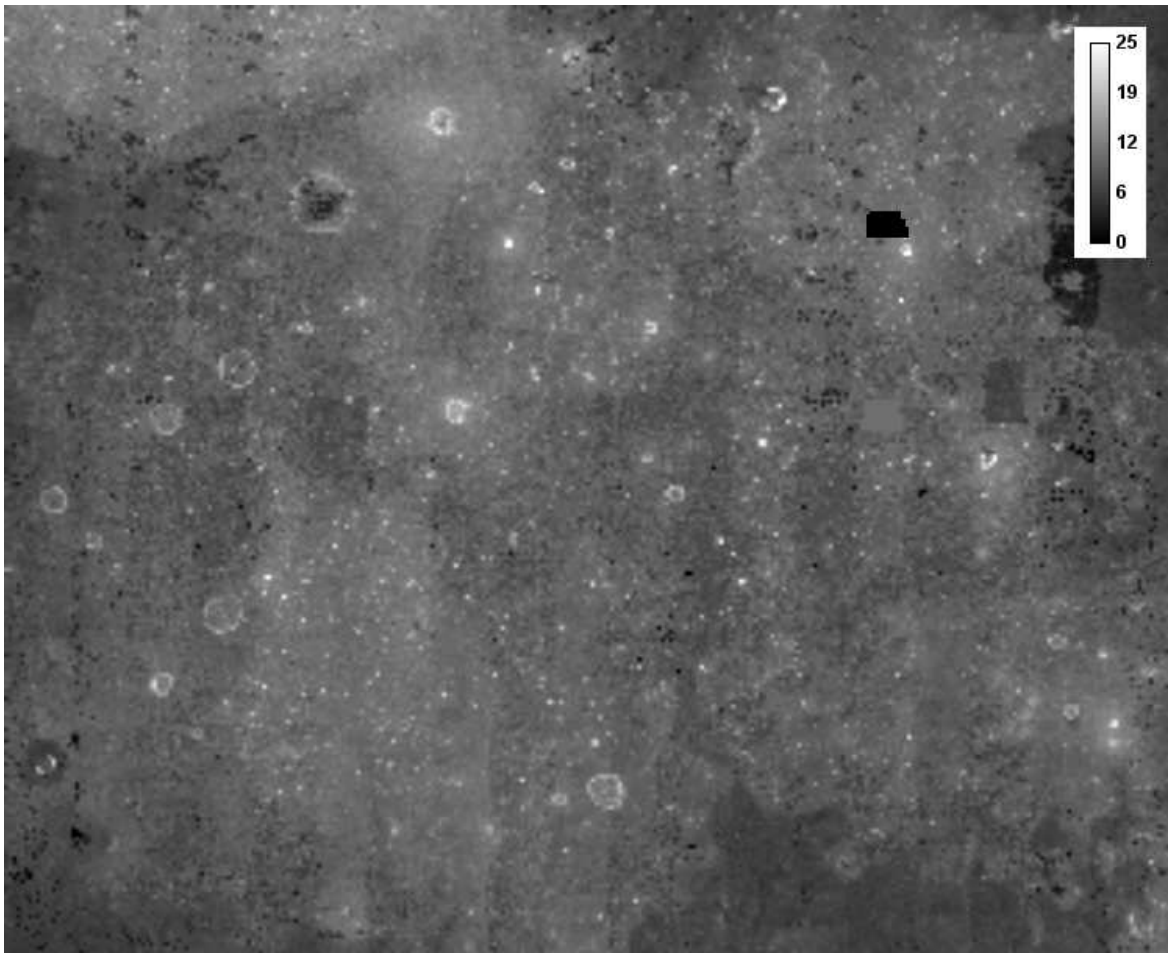

Figure 11 Iron map (wt %) of the Tranquillitatis basin

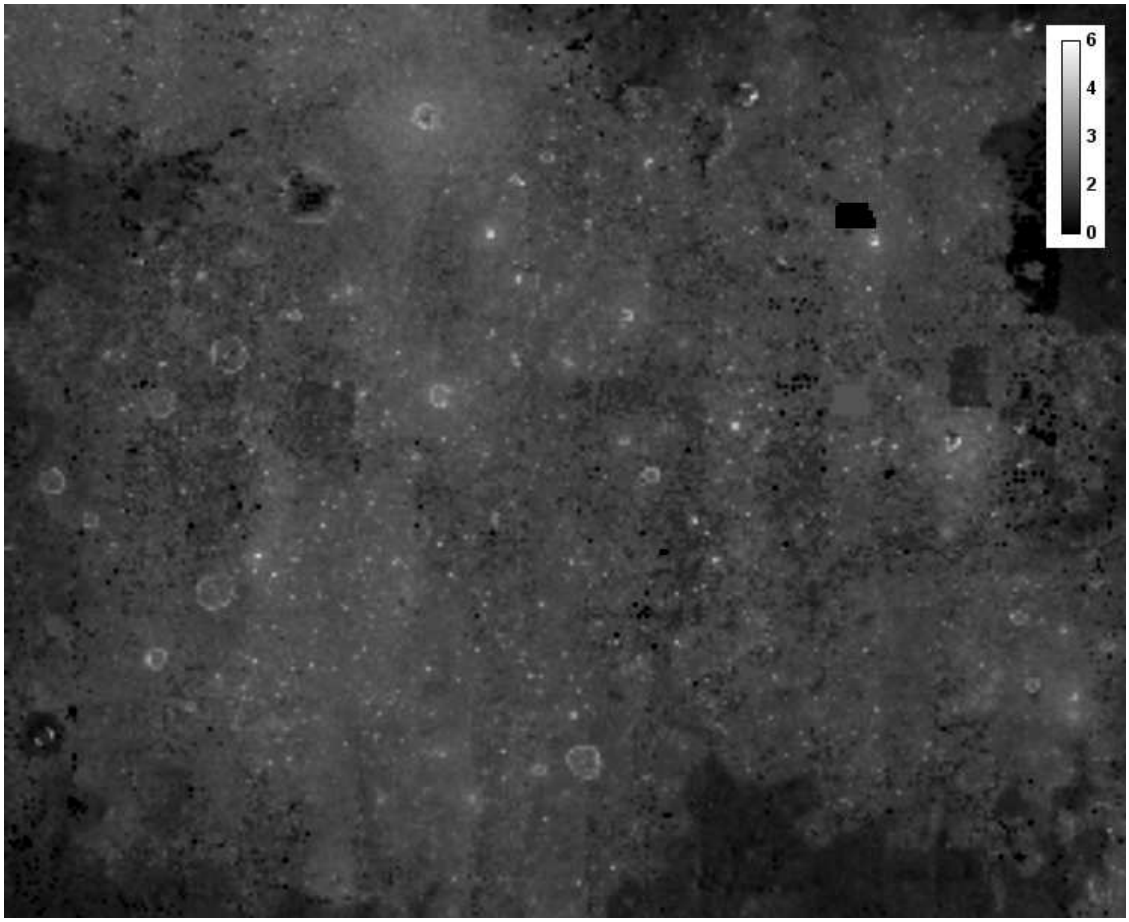

Figure 12 titanium map (wt %) of the Tranquillitatis basin

Stratigraphic evidence shows that for Dawes a lower titanium unit has been excavated from beneath spectrally bluer surface units.

A similar stratigraphic relationship concerning buried basalts is also identifiable for Arago crater (Fig. 9). The Arago floor exhibits spectral properties characteristic of non mare feldspathic materials. The walls and the central mountains of the crater show spectral properties characteristic of mare material characterized by titanium rich basalt (Al 7.3 wt%, Ti 3.6 wt%). Thus, the spectral character of the Arago ejecta (see Fig. 1, 7 and 9) is attributed to the excavation of underlying and less titanium-rich Th basalts and non mare feldspathic material according to Staid et al. (1996). This example confirms that the Th unit is stratigraphically older than the overlying Tvh basalts.

According to the spectral map and the basalt map (cf. Fig. 5 and 9) also Arago D and several small craters that occur within these deposits exhibit a distinct “blue halo” excavating Ti-rich mare basalt up to the surface (Ti 3.6 wt%). These small craters are interpreted to have re-exposed the Tvh-A surface basalts from just below Arago's ejecta deposit. Hence, high-titanium basalts (Tvh-A) were emplaced over a layer of lower Titanium basalts (Th). Subsequently, the Arago event has excavated underlying Th basalts and nonmare feldspathic materials from beneath producing the ejecta deposits around this crater. More recently, small impacts into Arago ejecta deposits produced dark haloed craters by exposing the Tvh-A surface unit from below the veneer of Arago ejecta that contains the older Th unit and nonmare feldspathic materials. The excavation of the Tvh-A unit by the small crater also demonstrates that the Arago event could not have been older than the emplacement of Tvh-A mare unit.

The corresponding petrographic maps shown in Figs. 7 and 9 indicate that the soil around the domes Arago α and β appears composed of highland-like material (blue) mixed with mare basalt. The highland contamination in the mare soil is more pronounced to the north than to the west, where the dome Arago β is localized.

According to the spectral maps prepared using the Clementine UVVIS+NIR dataset, the soil around Arago β displays a single absorption at 0.95 μm, indicating the presence of high and low Ca pyroxenes. In contrast, the spectral data of Arago α indicate the presence of an olivine component, characterized by a broad absorption band centered at about 1.10 μm.

Moreover, based on mapping the previously extracted spectral features to Lunar Prospector gamma ray spectrometer data, the abundances of the elements Ca, Al, Fe, Mg, Ti, and O were computed for both two examined lunar domes (Fig. 8). Accordingly the soil around two domes displays the same elemental composition (Ti 1.5 wt %, Fe 8.5 to 9.2 wt%) although the different color in ratio image (Fig. 4). It evidently reflects mixing between basalts and highland material.

On the other hand, Arago α and Arago β are characterized by complex surface detail, implying a variety of individual flow units, and show similar volumes and large diameters (cf. section 1). Hence, the overall formation conditions of the examined domes did not fundamentally change.

References

[1] Berezhnoy, A.A., Hasebe, N., Kobayashi, M., Michael, G. G., Okudaira, O., Yamashita, N. A. 2005. Three end-member model for petrologic analysis of lunar prospector gamma-ray spectrometer data. Planetary and Space Science**,** Volume 53, 11, 1097-1108.

[2] Evans, R. and Lena, R., 2010. Short Octave Program to Map Lunar Spectral Features: Application to Lunar Geologic Studies. Selenology Today, 18, 1-19.

[3] Evans, R., Wöhler, C., Lena, R., 2009. Analysis of Absorption Trough Features Using Clementine UVVIS+NIR Imagery. Lunar Planet. Sci. Conf., XXXX, abstract #1093.

[4] Evans, R., Wöhler, C., and Lena, R., 2009. Spectral mapping using Clementine UV-Visible-NIR Data Sets: Applications to Lunar Geologic Studies. Selenology Today, Vol. 14 pp. 1-70.

[5] Hiesinger, H., Jaumann, R., Neukum, G., and Head, J. W., 2000. Ages of mare basalts on the lunar nearside. J. Geophys. Res., 105- 29,239–29,275.

[6] Hiesinger, H., Head, J. W., Wolf, U., Jaumann, R., and Neukum, G., 2001. Lunar mare basalts: Mineralogical variations with time. 32nd Lunar and Planetary Science Conference (abstract #1826).

[7] Lena, R., Wöhler, C., Pujic, Z., Phillips, J., Lazzarotti, P., Bregante, M. T., 2005. An unlisted dome near crater Arago, TLO August 2005, pp. 5-9.

[8] Lucey, P. G., Blewett, D. T., Jolliff, B.L., 2000. Lunar iron and titanium abundance algorithms based on final processing of Clementine ultraviolet-visible images, J. Geophys. Res., 105(E8), 20,297–20,305.

[9] Pieters, C. M., 1978. Mare basalt types on the front side of the Moon: A summary of spectral reflectance data. Proceedings, 9th Lunar and Planetary Science Conference. pp. 2825–2849.

[10] Rajmon, D., and Spudis, P., 2001. Distribution and stratigraphy of basaltic units in Mare Tranquillitatis. Proc. Lun. Plan. Sci. Conf. XXXII, paper 2156.

[11] Rajmon, D., and Spudis, P., 2004. Distribution and stratigraphy of basaltic units in Maria Tranquillitatis and Fecunditatis: A Clementine perspective. Meteoritics & Planetary Science 39, 10, 1699–1720.

[12] Staid, M.I., Pieters, C. M., Head, J. W, 1996. Mare Tranquillitatis: Basalt emplacement history and relation to lunar samples. J. Geophys. Res., 101 (E10) 23,213-23,228.

[13] Wilhelms, D.E., 1987. The geologic history of the Moon. USGS Prof. Paper 1348.

[14] Wöhler, C., Lena, R., Lazzarotti, P., Phillips, J., Wirths, M., Pujic, Z., 2006. A combined spectrophotometric and morphometric study of the lunar mare dome fields near Cauchy, Arago, Hortensius, and Milichius. Icarus, vol. 183, no. 2, pp. 237-264.

[15] Wöhler, C., Berezhnoy, A., Evans, R., 2009. Estimation of Lunar Elemental Abundances Using Clementine UVVIS+NIR Data. Proc. European Planetary Science Congress, EPSC2009-263.

Spectral Study of the Eimmart Region

by Richard Evans, Raffaello Lena, Mardiña Clark and Christian Wöhler

Geologic Lunar Research (GLR) Group

Abstract

This paper presents a compositional and stratigraphic study of the Eimmart region using a Clementine UVVIS+NIR data set. Compositional analysis involved creation of spectra for pixel blocks of areas of interest, determination of elemental abundances, and generation of petrographic maps of the region. The study documents the geographic distribution and composition of ejecta materials from the Eimmart A impact within the region.

1. Introduction

Eimmart is a Nectarian era crater situated on modestly elevated terrain just to the northeast of the Mare Crisium rim (Head, 1978). Its eastern rim is excavated by the approximately Copernican age crater Eimmart A (based on its optical maturity values). Eimmart A has long been thought to be interesting compositionally and is felt to consist of a mixture of noritic and olivine rich material based on remote sensing (Pieters and Englert, 1993). To our knowledge, however, no detailed spectral mapping studies of this area have been conducted. We therefore attempted to better define and map the rock/ mineral composition of the Eimmart area and view results in the context of local stratigraphic relationships. In Figure 1, showing the embayment of Eimmart, and in the 950 nm Clementine image shown in Figure 2, Eimmart appears as the large central crater with Eimmart A present on its rim at about the 03:00 hr position. The dark form of Mare Anguis is shown extending obliquely just beyond the eastern border of Eimmart A.

The northeast margin of Mare Crisium occupies the lower left corner of the image.

Figure 3 illustrates the relationships between Eimmart, Eimmart A and the surrounding maria.

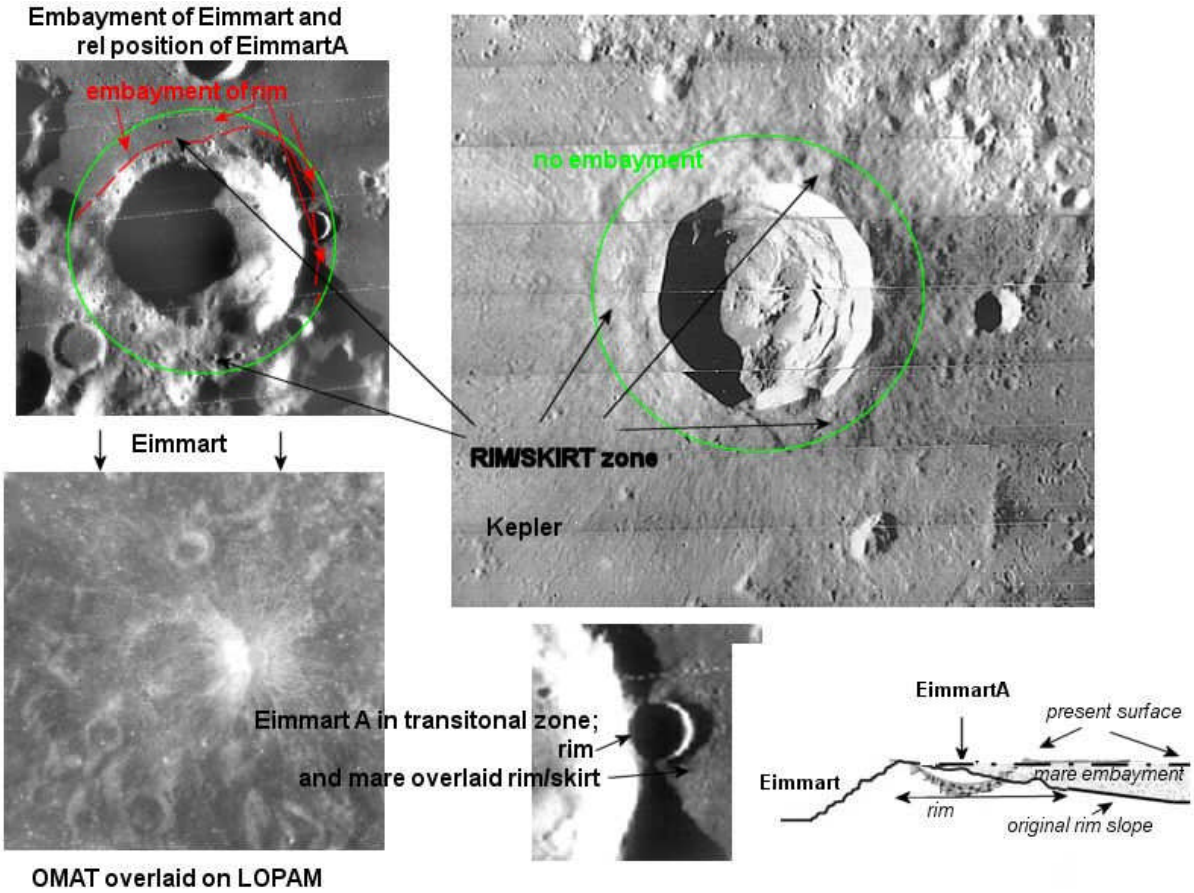

Figure 1: Embayment of Eimmart and transitional positioning of Eimmart A in rim/mare zone. The embayment of the outer rim of Eimmart crater shows that Eimmart formed before mare flooding of the surrounding surface, which is in contrast to other craters situated on mare surfaces, such as Kepler (upper right). The impact that formed Eimmart A occurred long after mare flooding.

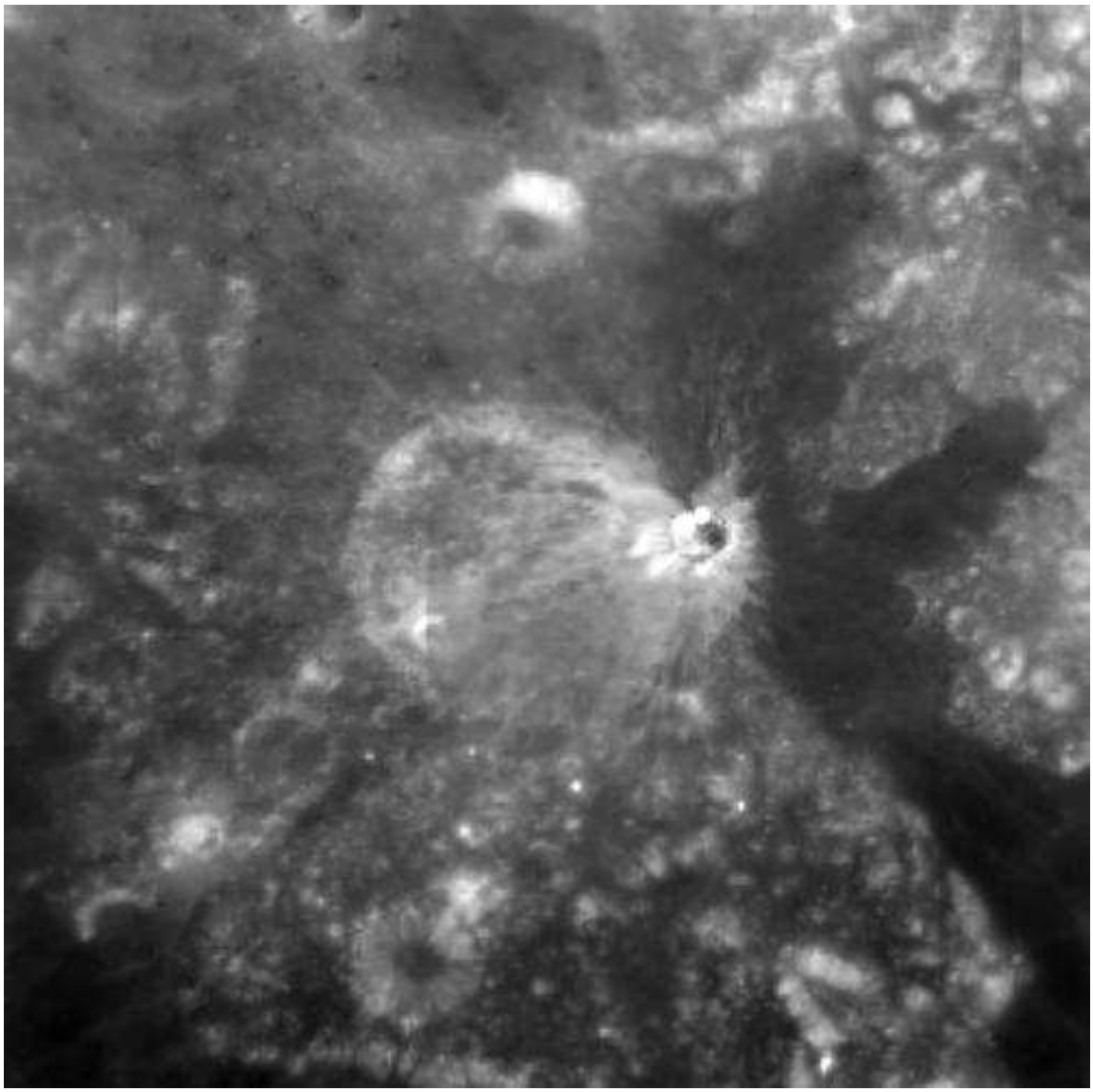

Figure 2: Eimmart area, Clementine 950 nm image. The original dimensions of this image were 500 x 498 pixels and (x,y) pixel coordinates referred to subsequently in the paper refer to features seen in the full scale image.

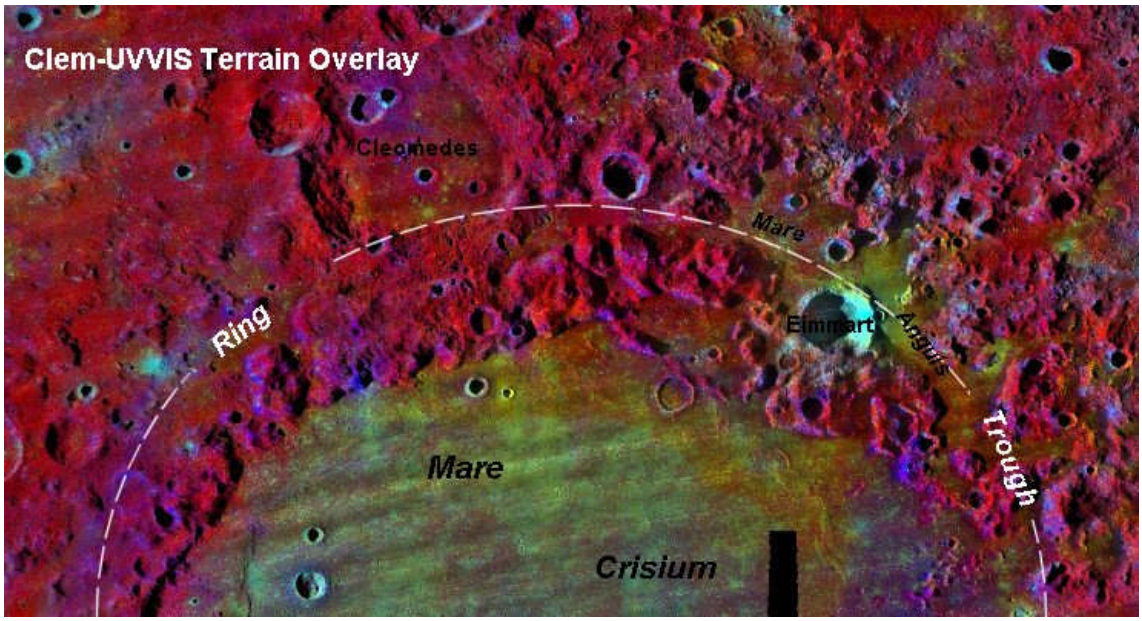

Figure 3: Region overview (Lunar Orbiter image with mafic ratio image as overlay).

2. Geologic History/Stratigraphy

Eimmart is a late Nectarian 46 km diameter crater emplaced upon a ring/trough zone in the NE part of Crisium basin post-dating the latter's formation. Eimmart was subsequently partially embayed on all but its southern flank by lavas forming Mare Anguis. Eimmart A is a 7 km crater emplaced upon the eastern rim/mare embayment zone of Eimmart. Based upon the morphology of the crater proper and its extensive, optically immature ejecta bisecting Mare Anguis, Eimmart A is considered late Copernican. The ejecta blanket of Eimmart A appears to contain both elements of Eimmart's rim material as well as extensively distributed excavations of the embaying mare material adjacent to Eimmart's rim. Preferential distribution of ejecta to the east suggests a slightly oblique impact, west to east.

Mare Anguis is an example of a ring-trough lava emplacement. This ring-trough emplacement, which is elevated by several hundred meters over Mare Crisum proper, is represented on the eastern and northern arc of the ring-trough by Mare Anguis, interrupted by the interposition of Cleomedes, then evident again to the southwest of

Cleomedes in another smaller region of unnamed ring-trough lava emplacements.

The age of these emplacements has not been previously suggested and it is classified as "undivided" by Head (1978).

However, (a) the anomalous higher elevations of these emplacements, combined with (b) a heavier mantling of highland material throughout the ring trough provinces than is found overlaying the annulus of the Mare proper, and (c) the presence of haloed craterlets in N and S Anguis and SW of Cleomedes with halo properties mineralogically consistent to those present in Eimmart A's extensive ejecta fan overlying central Mare Anguis, suggests an age consistent with the older lava emplacements designated by Head (Group IIb "Eimmart" basalts).

Furthermore, these basalt deposits appear as a discrete emplacement of the basalts of Mare Anguis and not a result of physical overflow of Mare Crisium lavas into these regions, although the opposite case, flow from these areas into Mare Crisium proper, has been postulated (Head, 1978; Wilhelms, 1973).

3. Studies of the Spectra of Pixel Blocks within the Eimmart Region

Analysis of the composition of the region was begun using the five-band UVVIS spectral method described by Tompkins and Pieters (1999). A total of ten pixel blocks were selected for various features of interest (Fig.4).

Interpretation of the spectra in accordance with the method described by Tompkins and Pieters (1999) indicates a composition of gabbroic noritic troctolitic anorthosite (GNTA type 2) for ejecta associated with Eimmart A and with a small crater on the floor of Eimmart at the 07:00 hrs position.

The remainder of the floor of Eimmart consists mainly of mature soil with a primarily anorthositic composition which may in part represent ejecta from other unrelated impact events. This type of material is scattered heavily over the surface of the adjacent Mare Anguis as well.

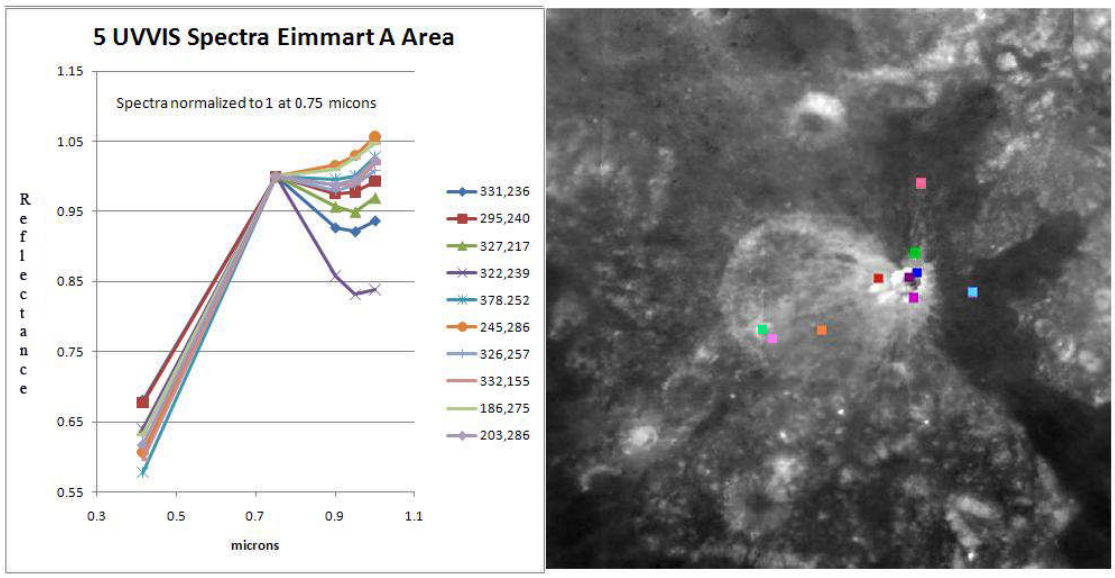

Figure 4: Five-band UVVIS spectra of Eimmart region.

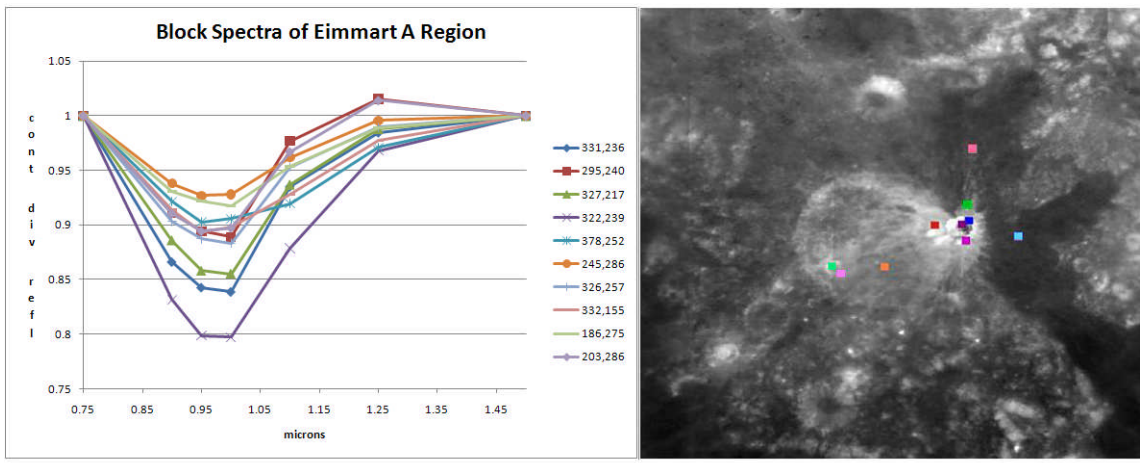

Figure 5: Continuum divided UVVIS+NIR spectra of Eimmart region.

The spectra were then represented as continuum divided UVVIS+NIR spectra as shown in Figure 5 for the same region.

The main area of interest was the ejecta associated with Eimmart A and the band depth here suggested a continuum of mafic content ranging from GNTA type 1 to the more mafic GNTA type 2 as suspected from the five-band UVVIS spectra. This method is discussed in more detail in Evans (2009). Because band depth can be affected by very high optical maturity (OMAT) values, an OMAT map was created for the region and is shown in Figure 6.

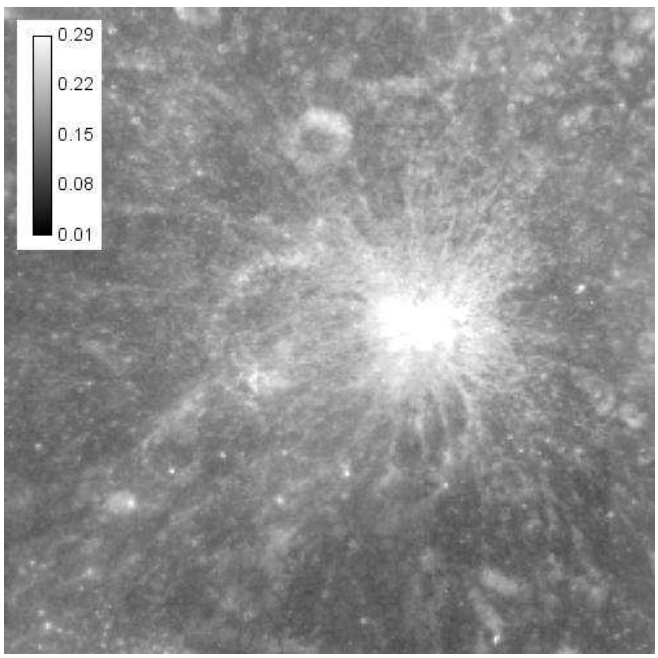

Figure 6: Optical maturity (OMAT) map of the Eimmart region.

The OMAT map suggests that Eimmart A is a relatively recent crater, perhaps approximately of late Copernican age. It has distributed its ejecta widely in the region and rays of ejecta appear relatively fresh. OMAT values are not high enough to affect band depth estimation for Eimmart A ejecta as they do not exceed a value of 0.4 and are indeed less than 0.3 except in the crater wall itself. More details on OMAT mapping in general is discussed by Evans et al. (2009) and a key reference is the work by Lucey (2000).

4. Spectral Parameter Mapping

Although the block pixel spectral studies provide a great deal of information, a spectral mapping of the region was conducted according to the method discussed by Evans and Lena (2010). This method uses Clementine UVVIS+NIR imagery to produce spectral band center, band depth and FWHM maps of the region of interest.

These maps indicate that the Eimmart A ejecta have a band center near 970 nm but with a wider than expected FWHM trough width in the low 300 nm range. This is suggestive of the presence of an admixed olivine component. Also, the band depth is rather mafic and not (for the most part) very anorthositic.

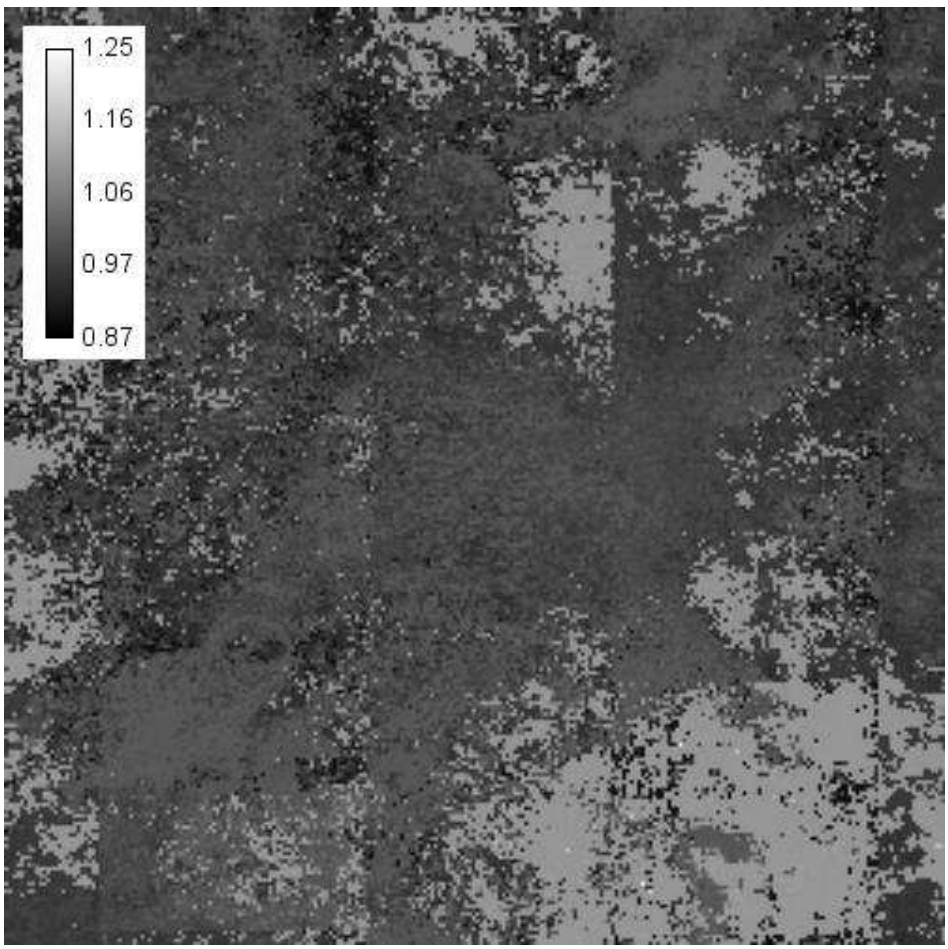

Figure 7: Band center map of the Eimmart region.

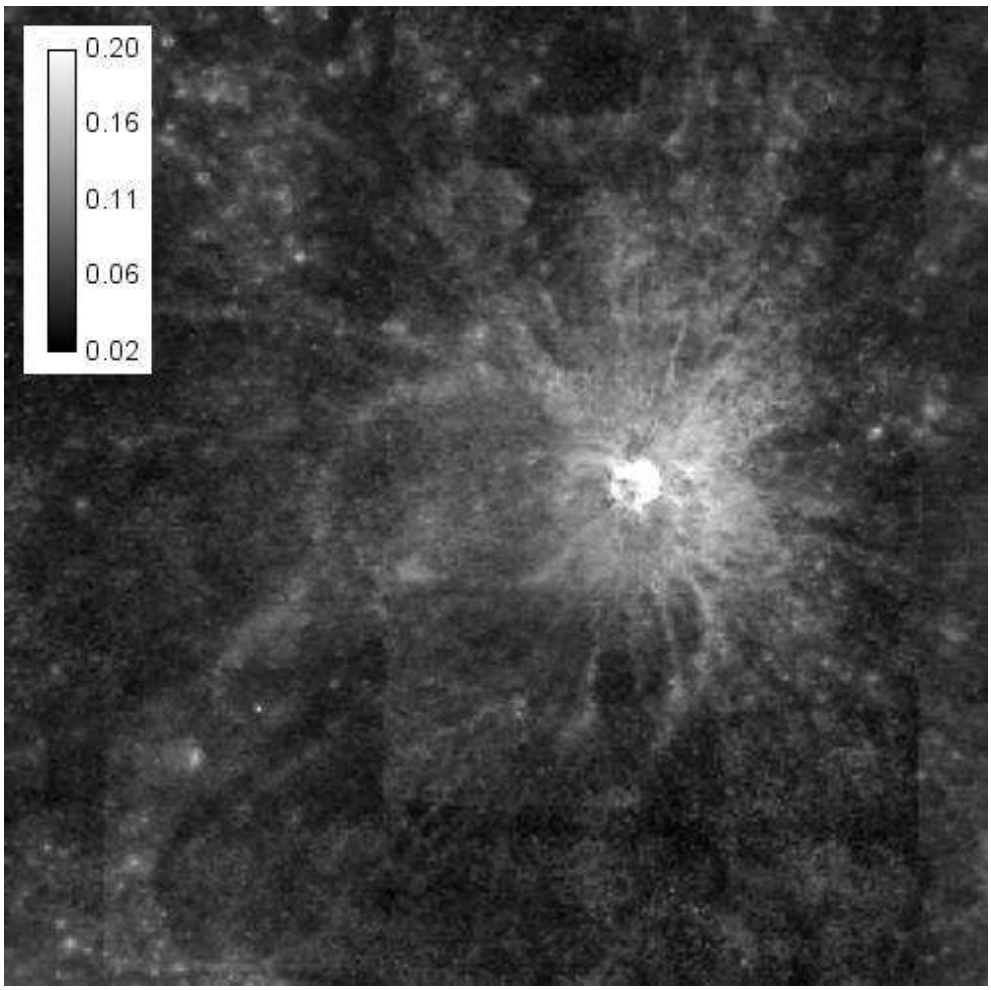

Figure 8: Band depth map of the Eimmart region.

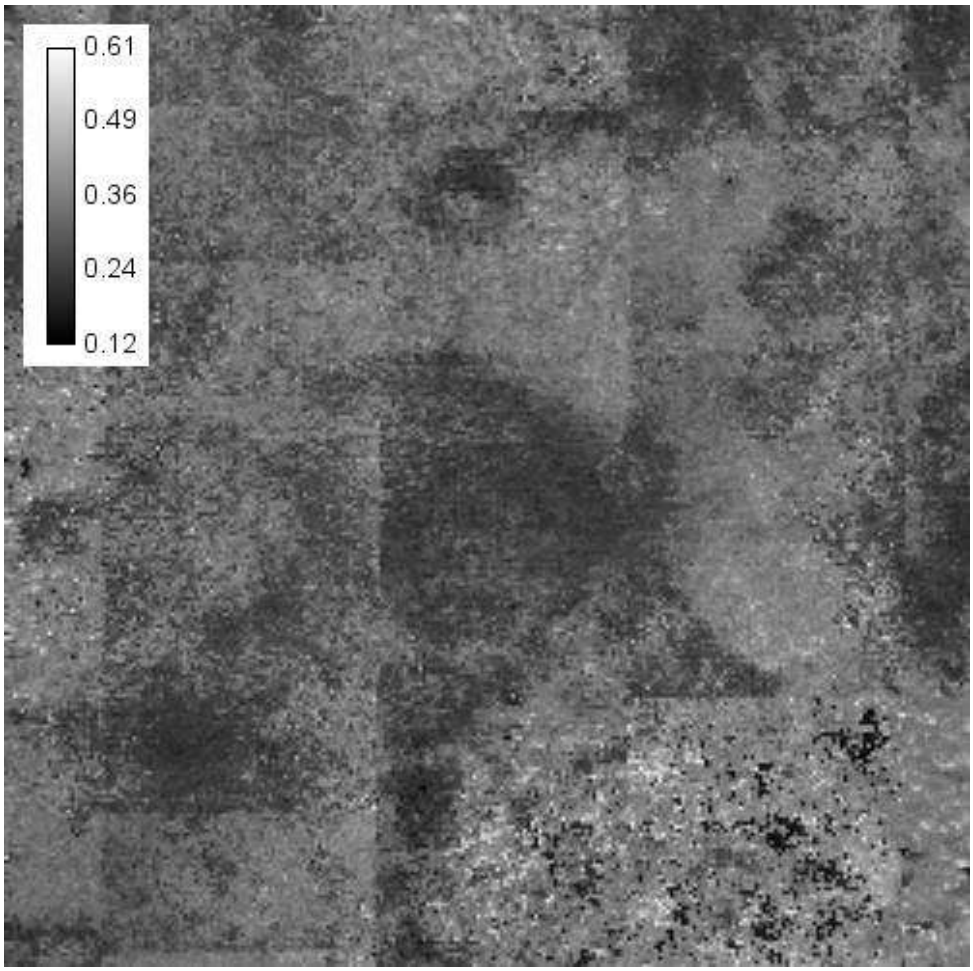

Figure 9: FWHM map of the Eimmart region.

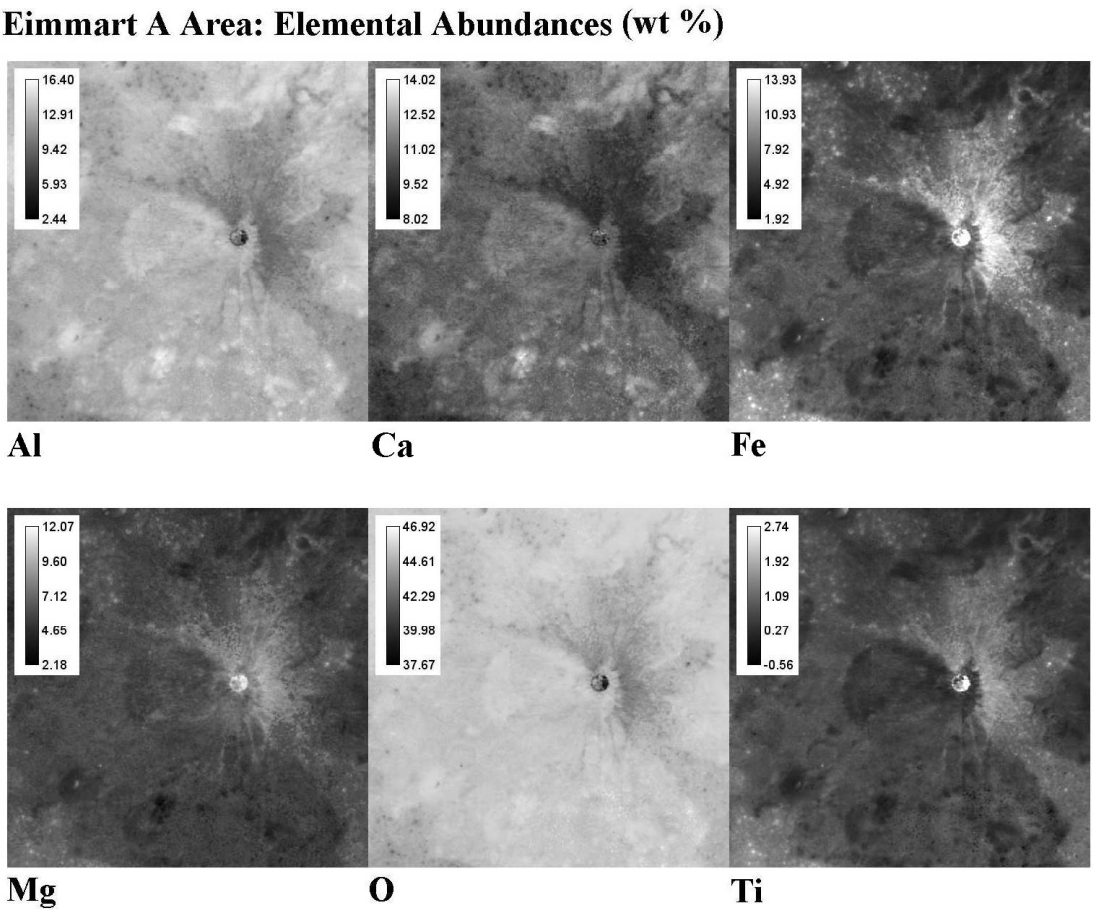

Figure 10: Elemental abundance maps of the Eimmart region. If the numbers on the calibration bars are difficult to read, the zoom feature of the PDF reader should be used.

4 Elemental Abundance Mapping

To better understand the composition of the region, elemental abundance maps were created according to the general method explained by Wöhler et al. (2009) except that four spectral maps (band center, band depth, FWHM, and slope) and their pairwise products were used rather than eight spectral maps and their pairwise products.

5. Petrographic Mapping

In order to put this elemental abundance information into a readily understandable geologic context, petrographic maps were created in which the relative fractions of the three endmembers mare basalt (red channel), magnesium-rich rock (green channel), and ferroan anorthosite (blue channel) were inferred from a ternary diagram in the space spanned by the Fe and Mg abundances to produce a petrographic map in which each of these rock/mineral types was defined in its respective color channel by their respective elemental abundance ranges. This approach is introduced by Berezhnoy et al. (2005) for petrographic mapping of elemental abundances measured by the Lunar Prospector spacecraft using gamma ray spectroscopy. The brightness and contrast of Figure 11 have been adjusted from the original map to enhance the image.

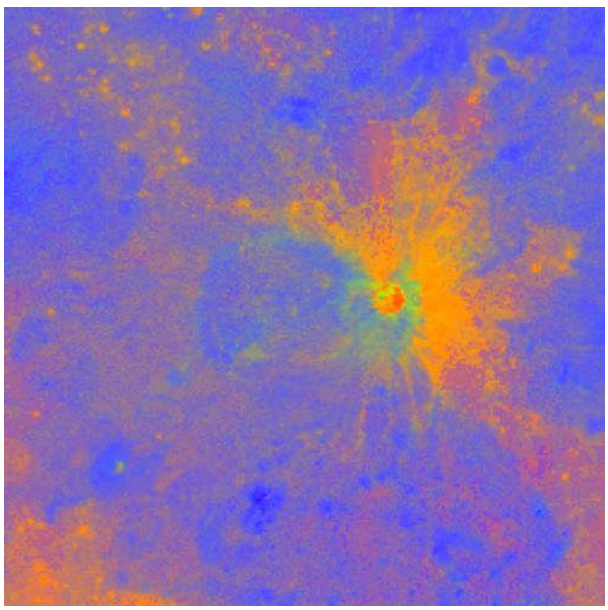

Figure 11: Petrographic map of the Eimmart region

(brightness and contrast enhanced).

Figure 12 is a higher resolution version of this map. The brightness and contrast are not enhanced and the map was made using all eight spectral parameters and their pairwise products as described by Wöhler et al. (2009). In this map all channels always sum to 255.

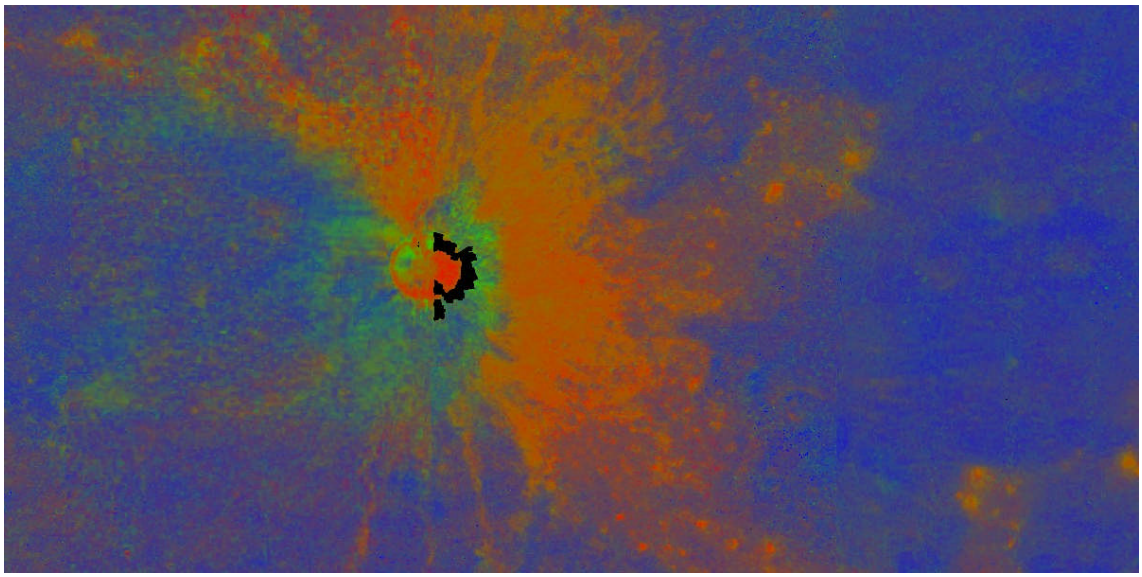

Figure 12: Petrographic map of the Eimmart region (high resolution).

To distinguish between different mare basalt types in the Eimmart region, we produced another petrographic map which displays the relative fractions of the three basalt endmembers titanium-poor mare basalt (red channel; 9.25 wt% Al, 1.6 wt% Ti), aluminous mare basalt (green channel; 14 wt% Al, 0.5 wt% Ti), and titanium-rich mare basalt (blue channel; 6.3 wt% Al, 3.6 wt% Ti). The relative fractions were inferred from a ternary diagram in the space spanned by the Al-Ti abundances.

Figure 13 displays a contrast-enhanced basaltic petrographic map of the Eimmart region and Figure 14 a higher-resolution version where no contrast enhancement has been applied. The maps reveal that the ejecta blanket of Eimmart A is not homogeneous but consists of titanium-rich (blue parts of the ejecta blanket in Figure 14) and titanium-poor (red-orange parts of the ejecta blanket) basalts as well as mixtures thereof (purple regions). Regions appearing in a green hue are not aluminous mare basalts but either

highland material (intense green) or mare basalt contaminated with highland material by lateral mixing effects (green/red colour). The surface of Mare Anguis consists mostly of the latter, "intermixed" type, where the small red dots correspond to fresh impact craters, whose ejecta blankets reveal the original composition of the titanium-poor mare basalt.

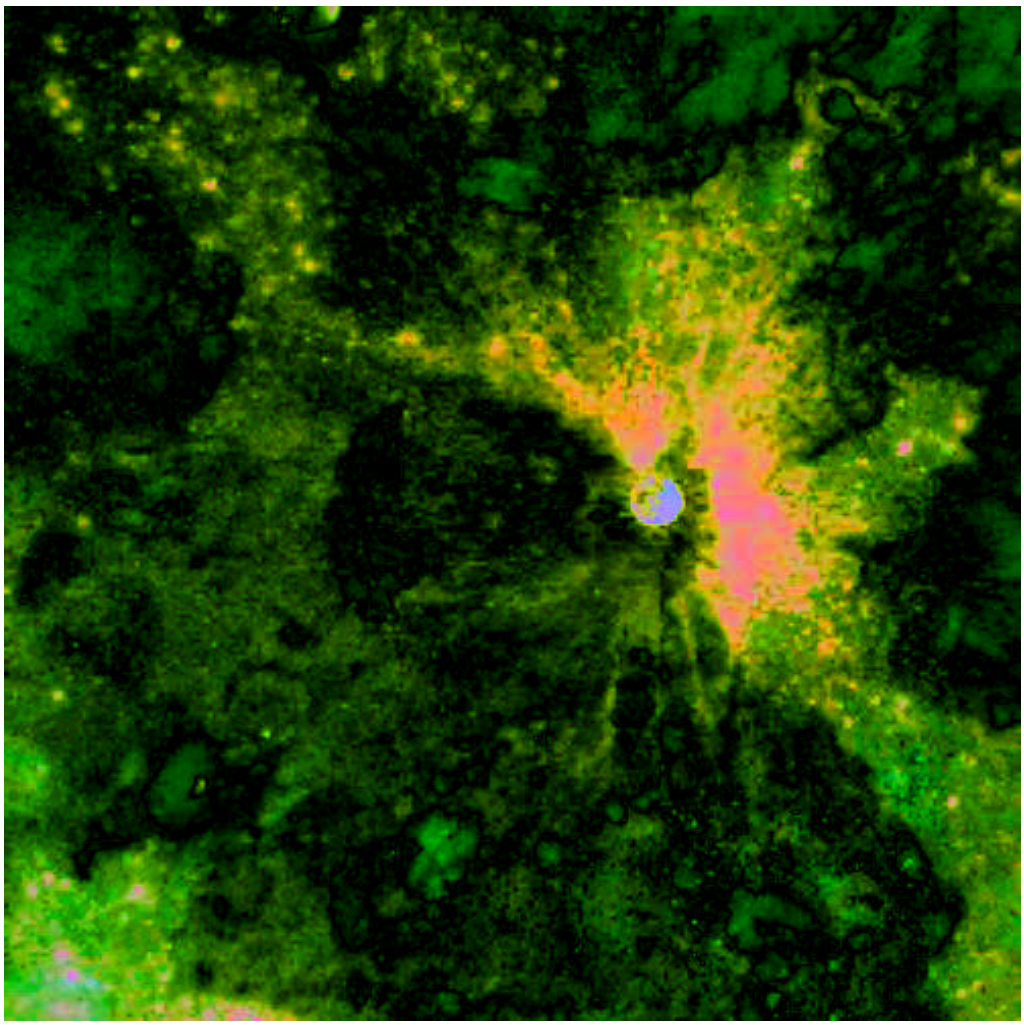

Figure 13: Basaltic petrographic map of the Eimmart region (brightness and contrast enhanced).

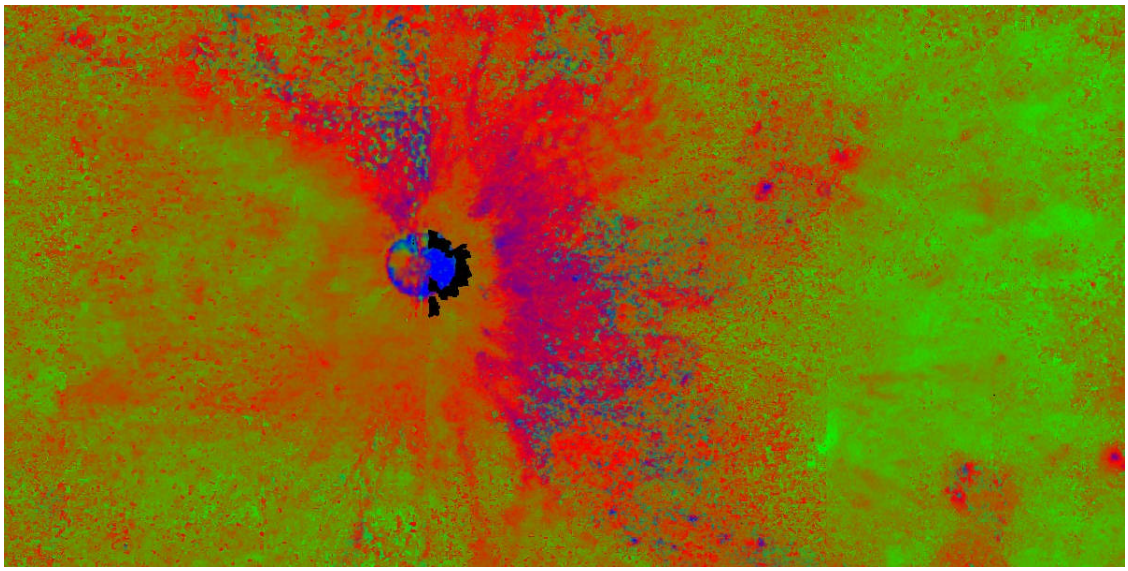

Figure 14: Basaltic petrographic map of the Eimmart region (high resolution).

5. Comparison of Elemental Abundance wt% Values with Pixel Block Areas

As an aid to interpreting the petrographic maps shown above, the elemental abundances in wt% for each pixel block area studied were assessed and are shown in Table 1 below.

The higher values for Fe and Ti, typical of basaltic composition, were inferred at several positions:

- (322,239) corresponding to the north wall of Eimmart A, with 18.3 wt% Fe, 2.8 wt% Ti, and 10.7 wt% Mg
- (378,252) corresponding to the eastern soil, orange in the petrographic map, with 11.1 wt% Fe, 1.4 wt% Ti, and 7.8 wt% Mg
- (332,155) corresponding to the northern soil, orange in the petrographic map, with 10.2 wt% Fe, 1.2 wt% Ti, and 7.7 wt % Mg

The lower values for Fe (< 9 wt%) and Ti (<0.8 wt %) correspond to higher amounts of Aluminum wt%, typical of highland composition (cf. Table 2). Higher amounts of Magnesium (8.9 wt%) are inferred in part of the Eimmart A wall (at pixel position 331,236).

Hence, the red to orange color in these petrographic maps indicates the presence of a mare basalt composition containing large amounts of clinopyroxenes. This basaltic unit was excavated by the impacts that originated smaller craters located in Mare Anguis, which appear surrounded by a red to orange patch. According to the petrographic basalt map they have excavated basalt with low Titanium content. Part of the floor of Eimmart A and the floor of smaller craters are also covered by this excavated mare basalt unit.

The blue coloration indicates very low iron rock, typically consistent with ferroan anorthosite or generally highland-like material (with a large amount of anorthositic rocks) appearing green in the petrographic basalt map. Note that the high OMAT value (larger than 0.35) of part of the inner wall of Eimmart A makes it impossible to interpret elemental abundance values or to interpret petrographic map pixels for it.

The green color of the ejecta blanket surrounding Eimmart A indicates the presence of magnesium- rich rock and is sensitive to the presence of olivine. A second, smaller Mg-rich rock (green) patch appears to be ejecta of a smaller crater inside Eimmart. Hence it demonstrates the presence of a sub-surface body of Mg-rich rock material under Eimmart crater. It was excavated by the impacts that formed Eimmart A and by the impact that originated a small unnamed crater in Eimmart, and was spread around the newly formed craters.

From the spectral data in this restricted region, the higher-Ti basalt unit in central Mare Anguis originates from Eimmart A impact ejecta and likely better represents the actual subsurface composition of the Mare Anguis basalts than the adjacent less titanium-rich surface mare surface basalts which are admixed in part by feldspathic material and "contaminated" by highland ejecta. These areas have a yellowish orange to scarlet in color in the petrographic map and a reddish scarlet color in the basaltic map. The same effect can be seen in areas of small crater ejecta on the surface of Mare Crisium.

Table 1: Elemental Abundance Values for Pixel Blocks

Pixels	Al wt%	Ca wt%	Fe wt%	Mg wt%	O wt%	Ti wt%
331,236	12.0	10.9	10.1	8.9	44.2	0.383
295,240	13.4	11.3	6.8	6.5	45.3	0.414
327,217	12.4	10.8	8.7	7.9	44.7	0.711
322,239	7.9	10.4	18.3	10.7	40.9	2.75
378,252	10.4	9.6	11.1	7.8	44.0	1.4
245,286	12.7	10.9	7.4	6.3	45.1	0.721
326,257	13.3	11.1	7.0	6.9	45.2	0.418
332,155	11.0	9.9	10.2	7.7	44.2	1.23
186,275	13.9	11.5	5.8	5.6	45.5	0.313
203,286	12.9	11.0	7.6	7.1	45.0	0.587

Table 2: Typical elemental composition of mare and highland regolith (extracted from General Dynamics/Convair study under contract to NASA)

wt%	Ca	Al	Fe	Mg	Ti	O
Highlands regolith	10.7	13.3	4.87	4.55	0.31	44.6
Mare regolith	7.88	6.97	13.2	5.76	3.1	41.7

6. Petrographic Mapping of the Crisium Region

Eimmart A is placed within the context of the larger Mare Crisium area and therefore standard petrographic maps (R/G/B = mare basalt/Mg-rich rock/FAN) and maps discriminating between several basalt compositions were made to examine similarities between Eimmart A and this larger area. The basaltic maps were created based on differences in average titanium and aluminum content (cf. Section 5).

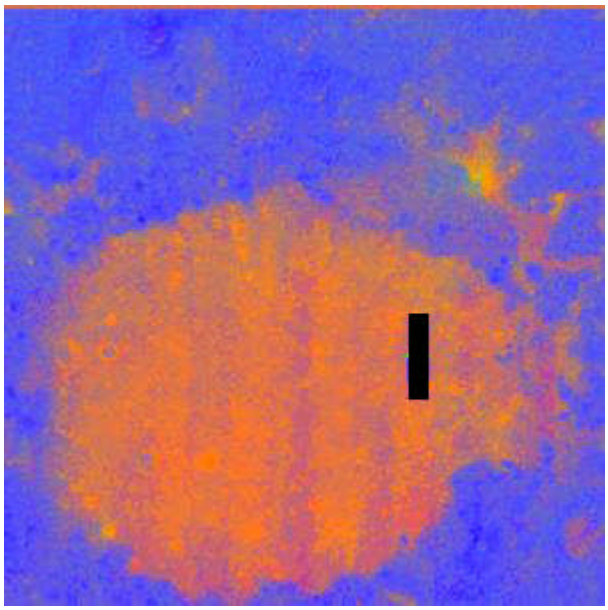

Figure 15: Standard petrographic map of Mare Crisium area.

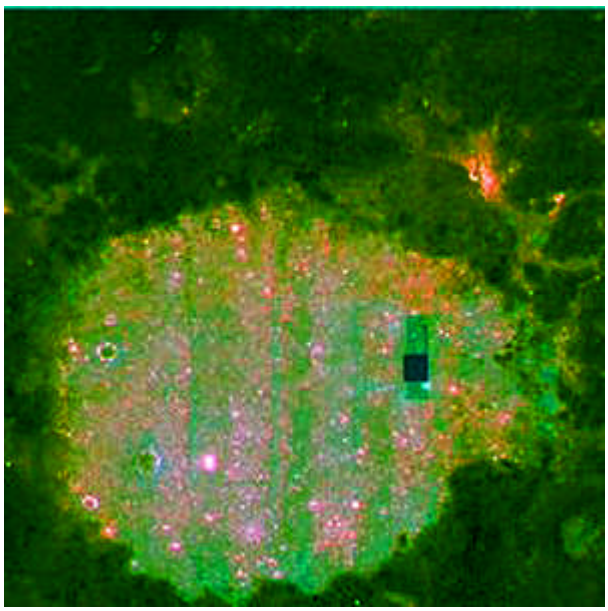

Figure 16: Basaltic petrographic map of Mare Crisium area

Most of the surface of Mare Crisium and Mare Anguis show an increased aluminium and decreased titanium content as compared to deeper mare surfaces exposed by small crater impacts or (in the case of northern Mare Anguis) deposited locally as the result of the Eimmart A impact. Presumably, this observation is due to lateral mixing effects leading to a "contamination" of mare surfaces by highland material. Figure 16 reveals two basalt species in Mare Crisium: a surface layer of variable thickness consisting of basalt admixed with highlands ejecta that is locally enriched in titanium by Eimmart A ejecta and perhaps some small crater ejecta; and likely a more titanium enriched underlying basalt that is free of highlands ejecta contamination. The southern part and center of Mare Crisium are covered by basalt with somewhat enriched Ti content due to Eimmart A ejecta, while the western, northern, and eastern rim zone are characterised by lower-Ti basalt.

7. Discussion

This study indicates that the Eimmart A impact, occurring at the junction of the rim of Eimmart crater and the immediately adjacent Mare Anguis, penetrated into both mare basalt and the pre-mare highlands material composing the rim of Eimmart. The mare material scattered over the surface of central Mare Anguis by the impact of Eimmart A provides the opportunity to study this material largely in the absence of contaminating surface dusting materials (and surface maturation effects) which are otherwise widespread over Mare Anguis and Mare Crisium. The Ti-enriched basalt unit is probably stratigraphically older than the overlying less titanium-rich surface basalts which are admixed with feldspathic highland ejecta. Surface maturation and highland contamination make this a difficult assessment. The elemental abundance values and petrographic maps of the crater wall of parts of Eimmart A itself are difficult to interpret because of their very high OMAT values (larger than 0.35) but a large part of the crater wall has lower OMAT values between about 0.30 and 0.32.

The present study also indicates that the Eimmart A impact penetrated into the rim of Eimmart and deeper highlands material of the basin ring crest/slope that Eimmart impacted upon. This event distributed pre-mare highlands material in a fairly circumferential halo zone immediately adjacent to the crater (skirt zone) around the crater. This highlands material is rich in aluminum, calcium, and magnesium but poor in iron and titanium. The composition of the halo or skirt zone, which appears greenish in the standard petrographic mapping, is consistent with GNTA type 2 material both in its elemental abundance wt% values and in the shape of its five-band UVVIS spectral curve.

Similar highlands material is also exposed by a smaller crater impact site on the floor of Eimmart crater and likely extends under a fairly broad area around Eimmart. This compositional information can also be viewed more qualitatively in the context of the maturation ratio image shown in Figure 17.

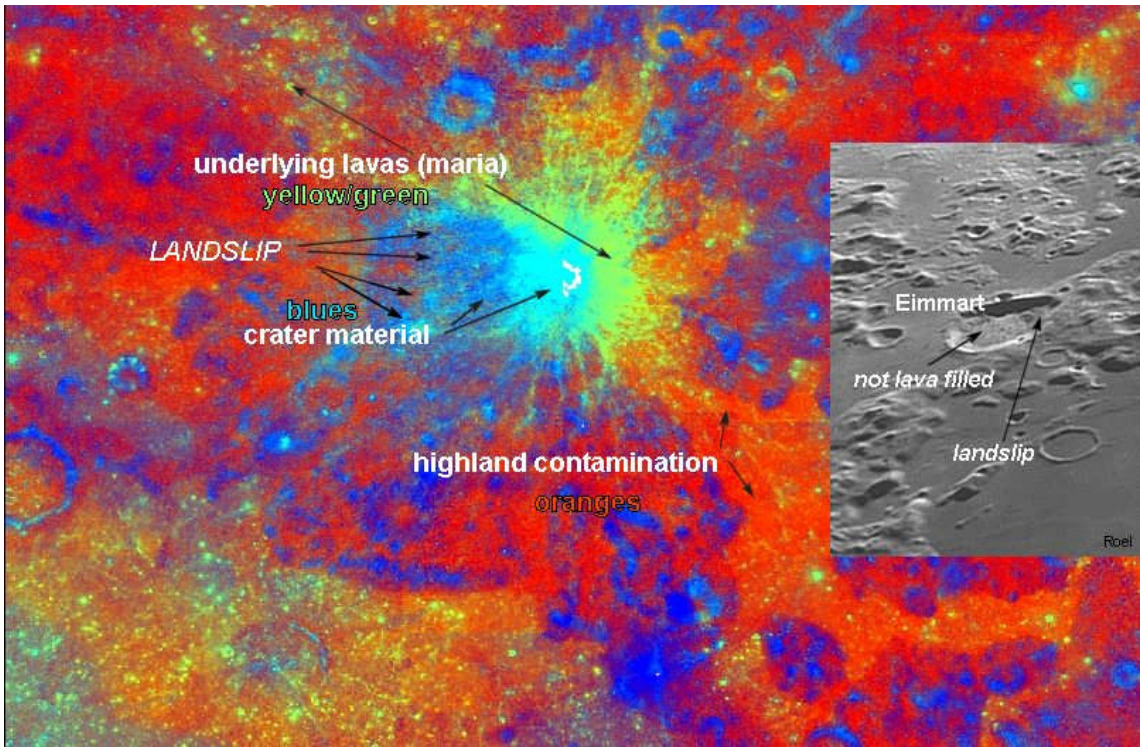

Figure 17: Maturation Ratio Image Graphic

As indicated in the inset, Eimmart crater proper is positioned lower than the surrounding Mare Anguis and shows numerous landslips of a rubble-like texture. It is not lava filled, but rather filled with rubble material mainly from the crater walls and rim. Similar subsurface highlands material is not spectrally evident in petrographic maps at the Cleomedes impact site presumably because of the degree of surface maturation and or surface ejecta deposits present here and the lack of a more recent significant impact such as that produced in the rim of Eimmart by the Eimmart A impact.

Petrographic mapping based on variations in elemental abundances is a useful tool in studying the composition and stratigraphy of lunar features. In the present study, petrographic mapping clearly demonstrated compositional differences between more recent and older mare basalts and also revealed areas of the ancient underlying highlands basin crust. These compositional differences were supported by examination of continuum divided spectra of specific pixel blocks and by reference to elemental abundance maps generated during the study.

Figure 18 is a view of the Crisium/Eimmart area taken by one of the authors (R. Lena) through an 18 cm telescope. It provides an excellent overview of the geography of this region as viewed through a small high quality telescope. It is amazing, however, how much more detailed our understanding of the geology of the terrain becomes when this basic geographic view is enhanced by spectral and petrographic mapping techniques discussed in this paper.

Figure 18: Crisium/Eimmart area taken by one of the authors (R. Lena) through a Maksutov Cassegrain 18 cm. Image made on June, 23, 2010 21:24 UT.

References

[1] Evans, R., Wöhler, C. and Lena, R., (2009) Analysis of Absorption Trough Features Using Clementine UVVIS+NIR Imagery. Lunar and Planetary Science Conference XXXX, abstract #1093.

[2] Evans, R., Wöhler, C., Lena, R., (2009) Spectra Mapping Using Clementine UV-Visible-NIR Data Sets: Application to Lunar Geologic Studies. Selenology Today #14 pp. 1 – 70.

[3] Evans, R. (2009) Spectral Studies of Aristarchus Using Clementine UVVIS/NIR (415 nm to 2000 nm). Selenology Today #12 pp. 22-38.

[4] Evans, R., and Lena, R., (2010) Short Octave Program to Map Lunar Spectral Features: Application to Lunar Geologic Studies. Selenology Today #18, pp. 1-28.

[5] Head, J.W., Adams, J.B., McCord, T.B., Pieters, C., Zisk, S., (1978) Regional Stratigraphy and Geologic History of Mare Crisium. In *Mare Crisium: The View from Luna24*. (Pergamon Press, NY) pp. 43-74.

[6] Lucey, P.G., Taylor, J., Hawke, B.R., (2000) Global Imaging of Maturity: Results from Clementine and Lunar Sample Studies. Lunar and Planetary Science Conference XXIX, abstract #1356.

[7] Pieters, C.M., and Englert, P.A.J., (1993) Topics in Remote Sensing 4. Remote Geochemical Analysis: Elemental and Mineralogical Composition. Chapter 14, Compositional Diversity and Stratigraphy of the Lunar Cruse Derived from Reflectance Spectroscopy. Cambridge University Press ISBN 0-521-40281-6, pp. 309-316.

[8] Tompkins, S. and Pieters, C.M., (1999) Mineralogy of the lunar crust: Results from Clementine. Meteoritics and Planetary Science, vol. 34, pp. 25-41.

[9] Wilhelms, D. (1973) Geologic History of the Moon. Available online at:

http://ser.sese.asu.edu/GHM/

[10] Wöhler, C., Berezhnoy, A., Evans, R., (2009) Estimation of Lunar Elemental Abundances Using Clementine UVVIS+NIR Data. European Planetary Science Congress, abstract #263.

Searching for lunar dome candidates using LTVT

by Maurice Collins

Palmerston North, New Zealand

Introduction

I have been using Jim Mosher's Lunar Terminator Visualization Tool (LTVT) for a number of years now and I have been exploring new ways it can display the Moon to give a better understand the lunar topography.

One potential application of LTVT is in the searching for new lunar dome candidates. Features suspected of being a dome could then be checked out using telescopic imagery. Visual and telescopic imagery verification is absolutely necessary as the resolution of the LOLA dataset is insufficient at present to describe any small features seen in complete high resolution detail. But its greatest potential use would be in directing observations to regions of interest for further study.

Application

The strength of this tool is in its ability to bring out low relief features across the whole of the image in the latest version, rather than waiting for the terminator to cross a feature of interest. So a wider area of the lunar surface can be studied at terminator lighting.

This will allow for the searching and possible discovery of low relief features such as lunar domes, over a wider area than just along the region of the current terminator. These candidate domes can then be specifically imaged to see if they are in fact domes and not just a raised wrinkle ridges or hills for example.

The resolution of the LOLA is limited near the equator due to orbital overlap, but is greatest near the South Pole. But this should improve as the mission of LRO gathers more data. The best resolution dataset is currently the LOLA 64 samples per degree available from the LTVT download site (http://ltvt.wikispaces.com/Sources+of+Planetary+DEM+Data). A higher resolution dataset should be released shortly, perhaps by the time you are reading this.

One unique feature of LTVT is its ability of putting the sun anywhere in the lunar sky. There is an option that allows the altitude and azimuth of the sun in the lunar sky to be specified. So if say 180 degree azimuth and 1.5 degree elevation is entered, we can get a

view of the displayed Moon's surface with the sun in the south casting shadows perpendicular to the normal direction of east and west. This may also allow previously unnoticed features to be discovered that are not normally lit by the sun in this way (Collins, 2010; Wood, 2010).

Also, different overlays can be combined with the DEM data to show the relationship of topography and elevation colours or geology among many others. The easiest ones to overlay are those textures that came with Virtual Moon Atlas (http://www.ap-i.net/avl/en/start). Just navigate to the VMA textures folder on your computer hard drive (under C:\Program Files\VirtualMoon\Textures) when setting up the file associations option in LTVT to point to the textures. Other textures have also been used that are freely downloadable through the LTVT Wiki site http://ltvt.wikispaces.com/Texture+Files.

Results

I have done some preliminary checking of known domes against the LTVT LOLA dataset. I have also searched a region (Mare Frigoris) to see what I could detect, then checked what was seen in the simulation against the Consolidated Lunar Dome Catalog (CDLC) (http://digilander.libero.it/glrgroup/consolidatedlunardomecatalogue.htm) and found it recorded some of the domes found there. The Consolidated Lunar Dome Catalogue contains all lunar domes which have been studied in detail by the GLR group and for which reasonably accurate morphometric properties could be determined. The catalogue is continuously updated according to ongoing observing and modelling activities.

The LOLA dataset has limitations of resolution in different sections of the Moon. There is higher resolution near the poles as the orbit is polar and covers the same regions repeatedly. It has much less resolution near the equator. In the Kaguya DEM data there are inaccuracies as shown by Lena in Selenology Today #17 (Lena, 2010). Also the Kaguya DEM resolution is 16 samples per degree, equal to the LOLA 16 dataset. LOLA has a higher resolution with the 64 samples per degree so greater detail can be resolved on the LOLA digital terrain model when that dataset is loaded. Also Kaguya has some spikes and omissions of data causing peaks where there are none, and missing craters. I have not found any problems at present with the LOLA dataset. As the mission progresses the resolution of the dataset will improve further, but for now it has limitation on how much "zoom" magnification it will allow LTVT to be set to before there is no more useful data to resolve. At the equator the limit is around a zoom setting of 3 to 5. At the poles that can be upped to about a maximum of 30 for regions around Cabeus crater at an oblique angle, but much less for rectified vertical views. Oblique angles near the

equator also are better, with zoom of about 10 to 15 possible due to 'angle of sight' compression.

As a test, Raffaello Lena sent me his Lunar and Planetary Conference (LPSC) 41 paper abstract (Wöhler et al., 2010). This paper described two domes, one in Grimaldi and the other near Aristillus. I setup LTVT in normal display mode (with a terminator casting shadows like in the real Moon) to match the UT times of the images and compared the LTVT image output to that in the paper. The domes in both regions were easily visible in the LTVT images, which demonstrates that in principle domes could be detected with the LOLA 64 DEM in LTVT.

I then set about searching a region that has few known domes, that of Mare Frigoris. Since I was unfamiliar with dome locations, it acted as a good blind test region. I found one candidate dome, and upon checking the CLDC database (Lena and Wöhler, 2009), found it to be Archytas 2 located using LTVT at 2.71W 56.52N. Archytas 1 is also visible as a small ridge. There are several other high flat regions that could be domes in Mare Frigoris, or they could be regions raised between wrinkle ridges. A study of these domes has been undertaken by Lena et al (2008).

When higher resolution LOLA data becomes available for LTVT, even more detail should be resolvable. Height measurements of the domes should also possible. Shadow length and lunar radius measurements can be determined from cursor position to reference points.

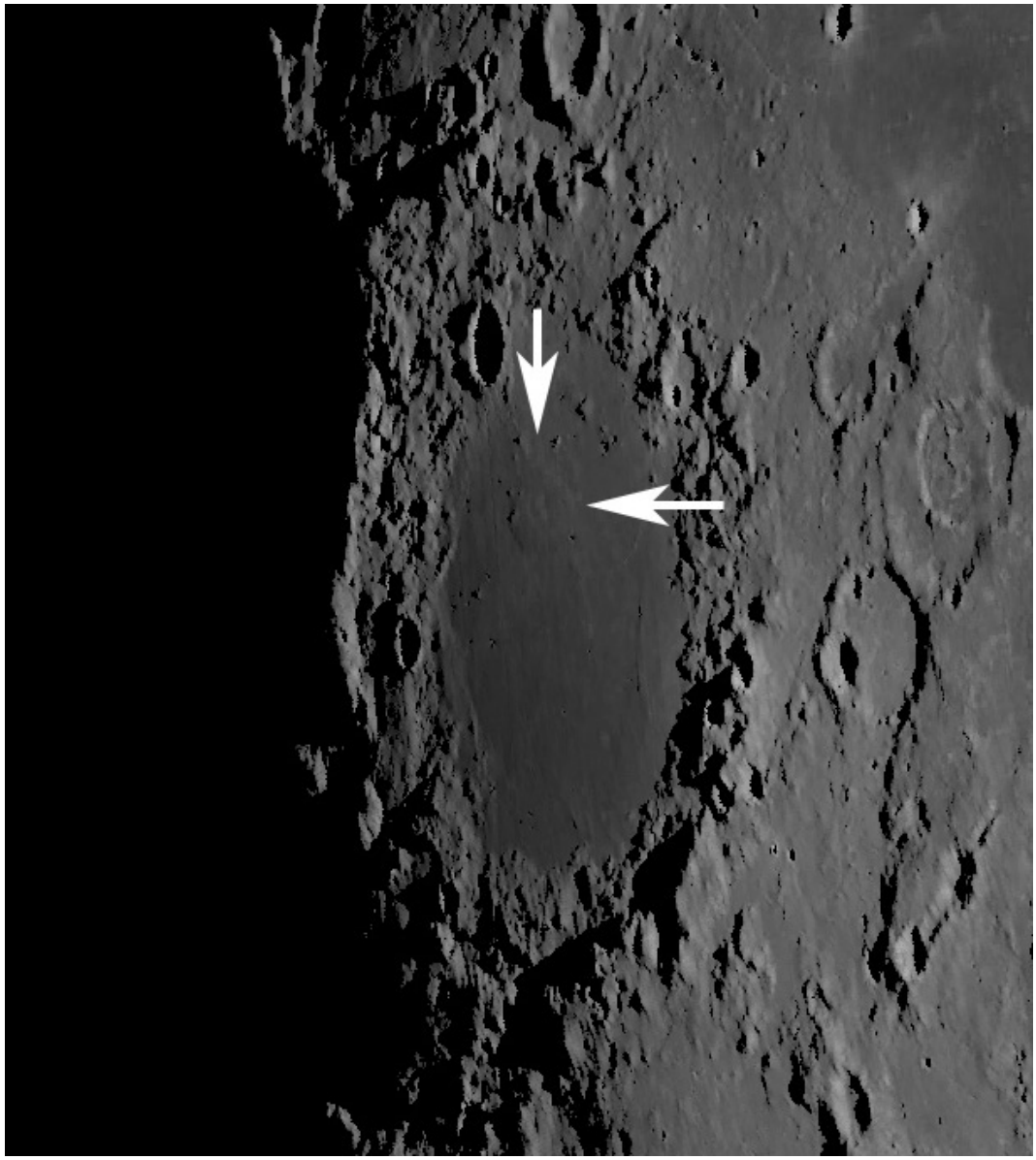

Figure 1. Grimaldi dome with LTVT

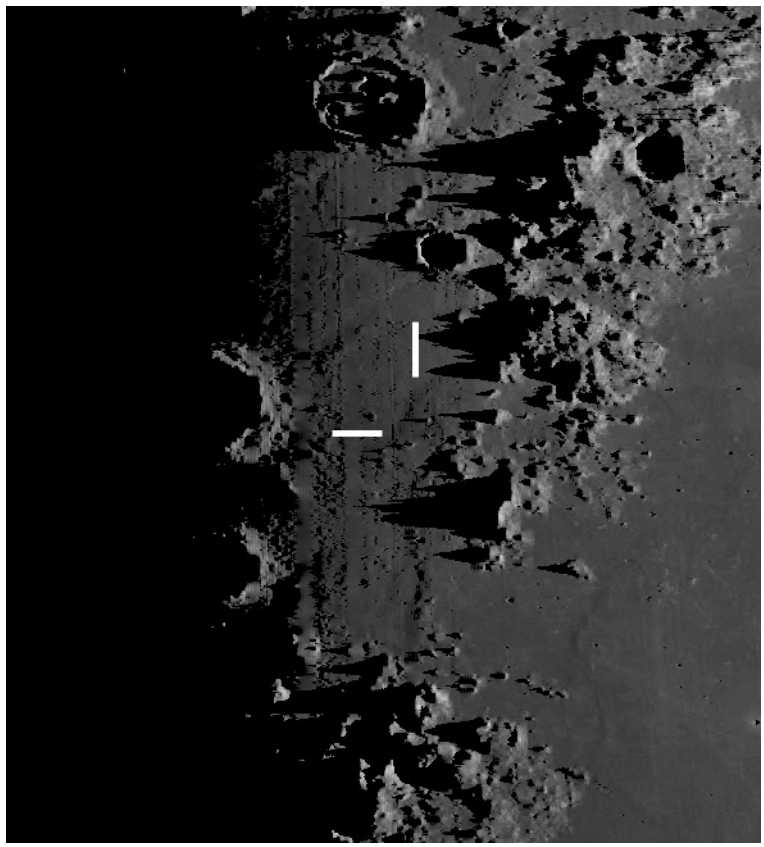

Figure 2. Aristillus dome with LTVT

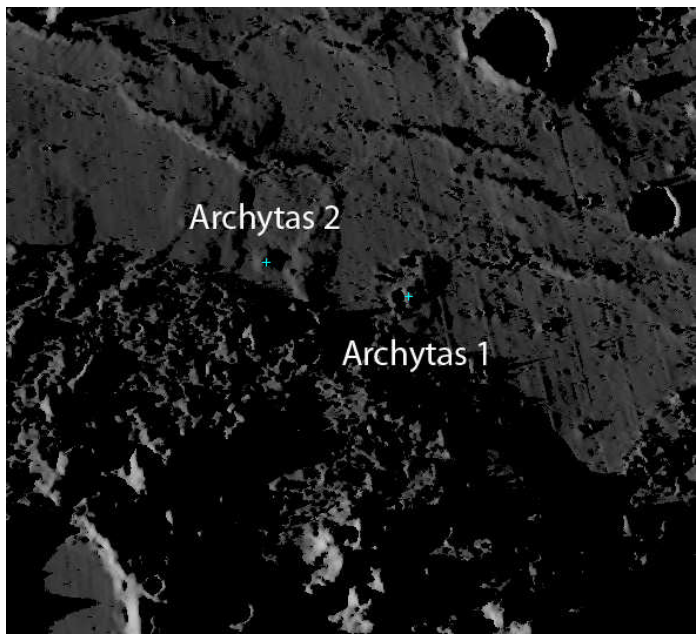

Figure 3. LTVT image of Archytas domes.

Summary

The LOLA dataset is a tool with great potential for lunar dome surveys and gives a place to start looking for new domes. All candidates must then be imaged under varying lighting conditions with telescopes to better understand their nature and to give better weight to their possible dome morphology. It may even be possible to study existing domes with LTVT under alternate lighting angles to better understand their morphology and geology. I hope this method over time, increases the number of lunar domes discoveries.

References

[1] Collins, M. (2010) Discovery of a Previously Unknown Imbrium Radial Ridge. *The Strolling Astronomer* - Journal of the Association of Lunar and Planetary observers, Vol. 52. No. 1. Winter 2010.

[2] Lena, R. (2010) Application in Lunar Studies of somulations and predicted from the Kaguya global DEM and LTVT software package. *Selenology today #17, February 2010*.

[3] Lena, R., and Wöhler, C. (2009) Consolidated Lunar Dome Catalog (CLDC): http://digilander.libero.it/glrgroup/consolidatedlunardomecatalogue.htm

[4] Lena, R., Phillips, J., Bregante, M.T., Lammel, S., Tarsoudis, G. (2008).

A study about two domes near craters C. Herschel and Archytas, and an effusive dome in Mare Frigoris. *Selenology Today 11*, 1-28

[5] LTVT (2010) *Lunar Terminator Visualization Tool*, http://ltvt.wikispaces.com/LTVT

[6] Virtual Moon Atlas http://www.ap-i.net/avl/en/start

[7] Wöhler, C., Lena, R., and Pau, K.C. (2010) Lunar Intrusive Domes on the Floor of Grimaldi and near Aristillus. LPSC 41, 1478.pdf http://www.lpi.usra.edu/meetings/lpsc2010/pdf/1478.pdf

[8] Wood, C. (2010) Lunar Missions & Amateurs. *Sky and Telescope*, May 2010, p51-52.

Focus On: measuring the elevation of the Plato's craterlets

by Raffaele Barzacchi and Raffaello Lena

Geologic Lunar Research (GLR) group

The image of Plato crater was taken on January 23, 2010 at 18:33UT (Fig.1 by R. Barzacchi). Barzacchi specifically increased the brightness to highlight better the shadows of the peaks of Plato. Within Plato, the first from west of craterlets solved of approximately 2km in diameter has a very strong shadow. It is clearly not present in the second, almost-twin but a little bigger. A project is the measure of its elevation. The image (Fig.1) was calibrated with the Lunar Terminator Visualization Tool (LTVT) using the ULCN 1994 list of control points. The reverse shadow length mode was used to determine the relative elevation of the measured craterlet.

Figure 1 image taken by Raffaele Barzacchi

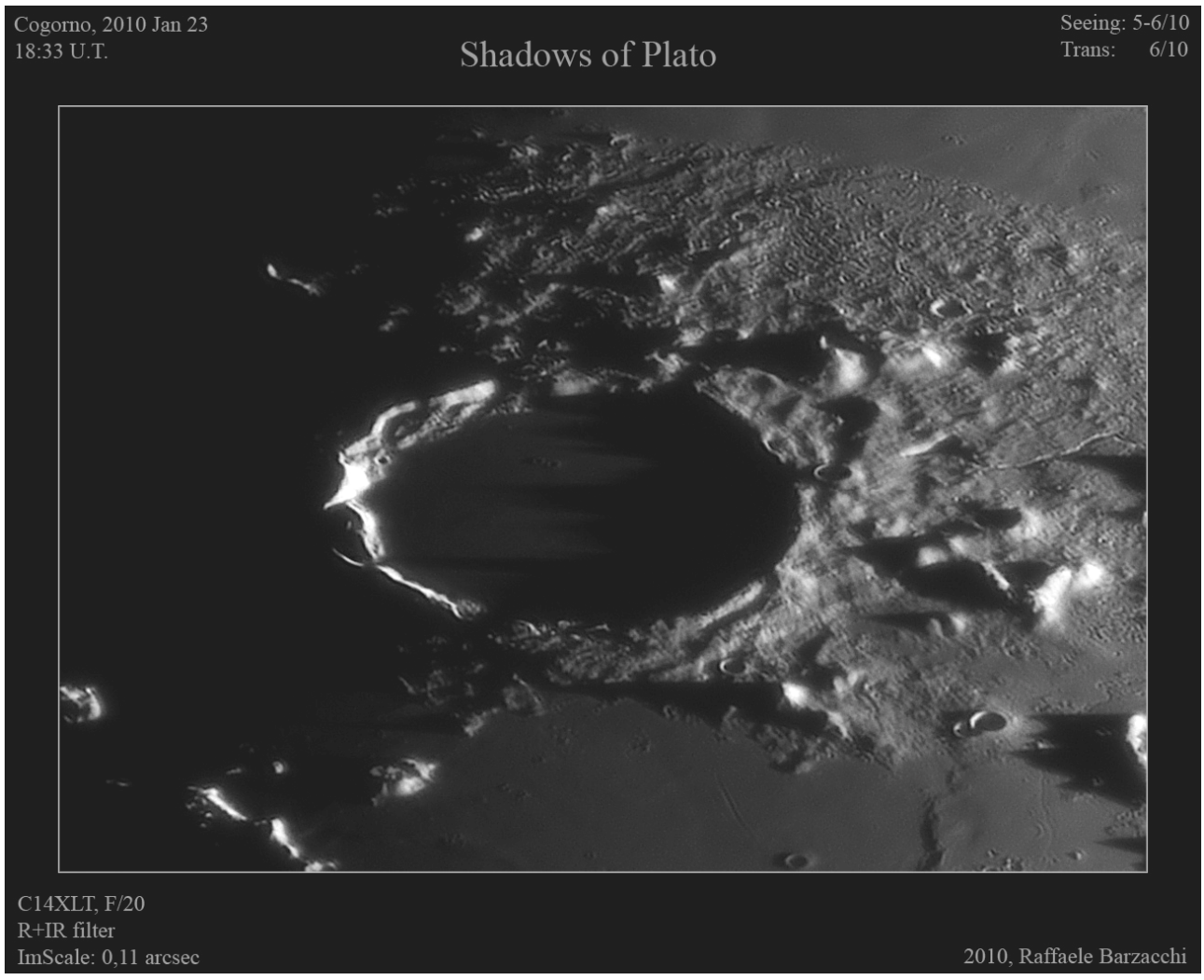

Estimated elevation and the lunar coordinates of the point of measurement were recorded from the LTVT data box. The measurements were then repeated several times and the greatest difference from the original readings were used to estimate the measurement error (Fig. 2 and the link below for lightened image so the mare details can be seen).

The difference between the rim of the craterlet and the soil was computed as 68 m ± 10 m. The elevation of the second craterlet, located to the east, was not measured because it displays a shadow rising on the rim of the western craterlet, thus the shadow length will be shorter (upward slope). Measurements of elevation of these craterlets such as Plato require multiple measurements. The error margin for the elevations represents the precision of the measurements, but additional measurements might be necessary to establish the true accuracy. Multiple images under varying light conditions would further elucidate the heigths of the two examined craterlets. The diameters of the two craterlets were computed as 1.97 ± 0.5 km and 2.17 ± 0.5 km for the western and eastern craterlet respectively.

Two examined features can be compared with preceding measurements, reported in Table 1 and in Fig.3. See also Fig.2 and the link
http://digidownload.libero.it/glrgroup/platoT.jpg

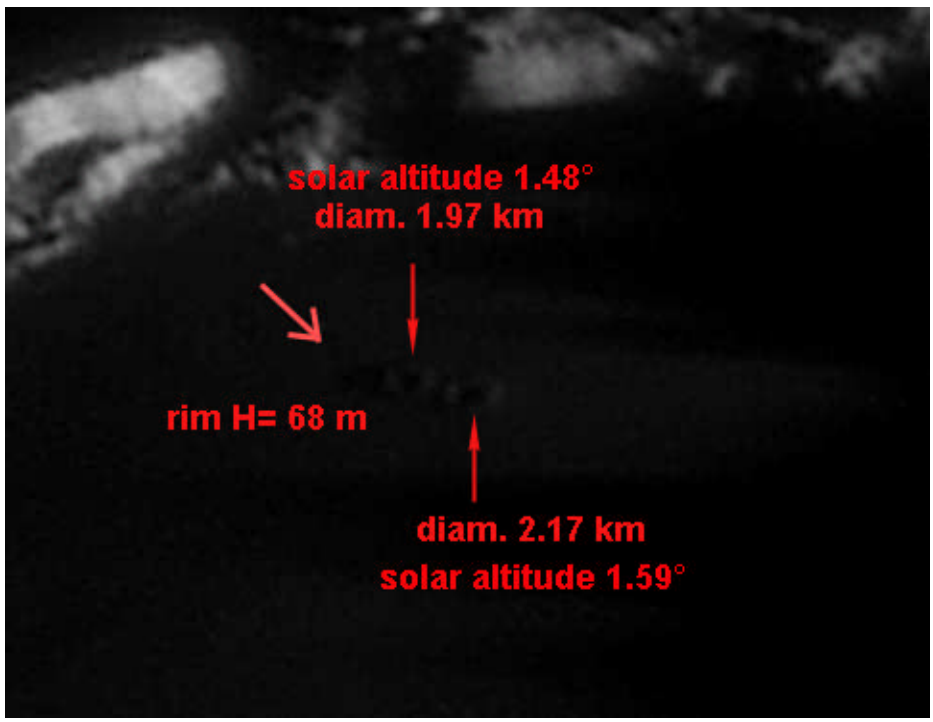

Figure 2

Table 1

Craterlet	Pickering	Wood	Knisely	Mosher (L.Orbiter)	Mosher (Clementine)	Lena and Barzacchi
1	1.3 (+)	2.0 (+)	2.4 (°)	2.24 (*)	2.24 (*)	2.17
2	0.9 (+)	1.7 (+)	2.1 (°)	1.98 (*)	1.94 (*)	1.97

(+) Wood, CA http://www.lpod.org/?page_id=632

(°) Knisely, D http://www.cloudynights.com/ubbarchive/showflat.php/Cat/0/Number/520616

(*) Mosher, J. http://the-moon.wikispaces.com/Plato+craterlets

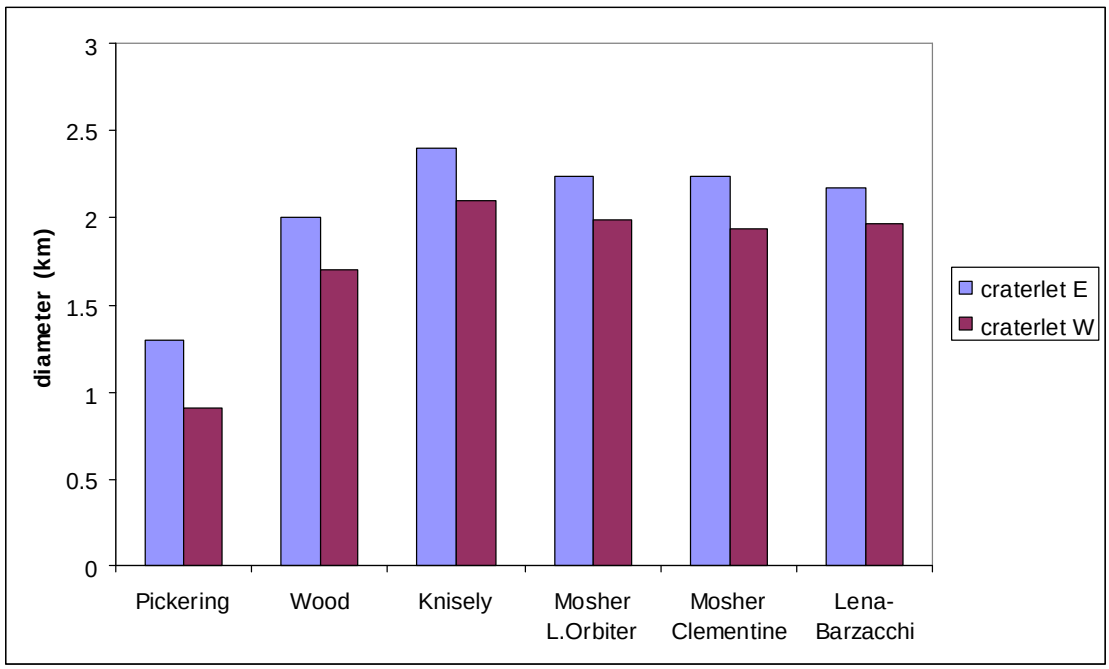

Figure 3